

# A Non Parametric Model for the Cosmic Velocity Field

E. Branchini<sup>1</sup>, L. Teodoro<sup>1</sup>, C.S. Frenk<sup>1</sup>, I. Schmoldt<sup>2</sup>,  
 G. Efstathiou<sup>3</sup>, S.D.M. White<sup>4</sup> W. Saunders<sup>5</sup>, W. Sutherland<sup>2</sup>,  
 M. Rowan-Robinson<sup>6</sup>, O. Keeble<sup>6</sup>, H. Tadros<sup>7</sup>, S. Maddox<sup>3</sup>, S. Oliver<sup>6</sup>,

<sup>1</sup>*Department of Physics, University of Durham, South Road, Durham DH1 3LE, UK*

<sup>2</sup> *Department of Physics, University of Oxford, Keble Road, Oxford OX1 3RH, UK*

<sup>3</sup> *Institute of Astronomy, University of Cambridge, Madingley Road, Cambridge CB3 0HA, UK*

<sup>4</sup> *Max Planck Institut für Astrophysik, Karl-Schwarzschild-Straße 1, 85740 Garching, Germany*

<sup>5</sup> *Institute for Astronomy, University of Edinburgh, Blackford Hill, Edinburgh EH9 3JS, UK*

<sup>6</sup> *Imperial College of Science, Technology, and Medicine, Blackett Laboratory, Prince Consort Road, London SW1 2EZ, UK*

<sup>7</sup> *Department of Physics, University of Sussex, Falmer, Brighton BN1 9QH, UK*

2 December 2024

## ABSTRACT

We present a self-consistent nonparametric models of the local cosmic velocity field based on the density distribution in the PSCz redshift survey of IRAS galaxies. Two independent methods – both based on the assumptions of gravitational instability and linear biasing – have been applied. They give remarkably similar results, with no evidence for systematic differences and a RMS discrepancy of only  $\sim 70 \text{ km s}^{-1}$  in each Cartesian component of velocity. These uncertainties are consistent with a detailed independent error analysis carried out on mock PSCz catalogues constructed from N-body simulations. The denser sampling provided by the PSCz survey compared to previous IRAS galaxy surveys allows us to reconstruct the velocity field out to larger distances. The most striking feature of the model velocity field is a coherent large-scale streaming motion along a baseline connecting Perseus–Pisces, the Local Supercluster, the Great Attractor, and the Shapley Concentration. We find no evidence for back-infall onto the Great Attractor. Instead, material behind and around the Great Attractor is inferred to be streaming towards the Shapley Concentration, aided by the compressional push of two large nearby underdensities. The PSCz model velocities compare well with those predicted from the 1.2Jy redshift survey of IRAS galaxies and, perhaps surprisingly, with those predicted from the distribution of Abell/ACO clusters, out to  $140 h^{-1} \text{ Mpc}$ . Comparison of the real-space density fields (or, alternatively, the peculiar velocity fields) inferred from the PSCz and cluster catalogues gives a relative (linear) bias parameter between clusters and IRAS galaxies of  $b_c = 4.4 \pm 0.6$ . Finally, we compare the cumulative bulk flows predicted from the PSCz gravity field with those measured from the Mark III and SFI catalogues of peculiar velocities. A conservative estimate of  $\beta = \Omega_0^{0.6}/b$ , where  $b$  is the bias parameter

for IRAS galaxies, gives  $\beta = 0.76 \pm 0.13$  ( $1-\sigma$ ), in agreement with other recent determinations.

**Key words:** Cosmology: theory – galaxies: large-scale structure, large-scale dynamics.

## 1 INTRODUCTION

The art of modelling the cosmic velocity field, which originates from the desire to interpret observed deviations from a uniform Hubble expansion, has developed rapidly over the past few years. There are two main reasons for this. One is an increase in the quantity and quality of measured galaxy peculiar velocities. The other is the advent of near all-sky, flux-limited, redshift surveys that allow self-consistent theoretical predictions to be made with the requisite accuracy.

Although other possibilities have been proposed (e.g. Babul *et al.* 1994), the gravitational instability theory (Peebles 1980) has proven to be the most successful theoretical framework in which to interpret peculiar velocities in relation with inhomogeneities in the mass distribution. Early attempts to account for observed velocities within this general framework were rather simplistic due to incomplete knowledge of the distribution of galaxies in the local universe. Thus, simple parametric models were developed to account for cosmic flows in terms of infall onto one or more spherical overdensities like the Virgo Cluster, the Great Attractor or the Perseus Pisces supercluster (Davis and Peebles 1983, Lynden-Bell *et al.* 1987, Peebles 1988, Han and Mould 1989). The situation changed dramatically when statistically complete, near all-sky, redshift catalogues of galaxies were constructed as it then became possible to predict peculiar velocities directly, assuming that luminous objects trace the underlying density field in some fashion. Since then, several modelling procedures have been developed which are generally based on the simplifying assumption that the gravitating mass is distributed just like the tracer objects (galaxies or clusters), although the relative amplitude of the deviations from uniformity, usually called the bias, is taken to be a free parameter. In addition to this “linear bias model,” current methods also assume gravitational instability in the linear or mildly nonlinear regime (e.g. Yahil *et al.* 1991, Kaiser *et al.* 1991, Nusser and Davis 1994, Fisher *et al.* 1995b, Sigad *et al.* 1997), therefore requiring smoothing over scales where non-linear effects are important. This requires the additional assumption that smoothing a distribution that has evolved to a nonlinear state gives a result that can be modeled by linear or quasilinear evolution from smoothed initial conditions.

Because of their large sky coverage, the most extensively used redshift surveys are those based on the “Point Source Catalogue” (PSC) of IRAS galaxies (e.g. the 1.9 Jy survey of Strauss *et al.* 1990, the upgraded 1.2 Jy catalogue of Fisher *et al.* 1995a, or the deeper but sparser QDOT survey of Rowan-Robinson *et al.* 1990). Other catalogues containing different kinds of objects such as optically selected galaxies (e.g. Shaya, Tully and Pierce 1990, Hudson 1994, Baker *et al.* 1998) or clusters of galaxies (Branchini and Plionis 1996) have also been used to produce model velocity fields on scales up to  $200 h^{-1} \text{ Mpc}$ <sup>\*</sup>.

Comparison of a model velocity field with directly measured peculiar velocities provides a means to constrain the density parameter,  $\Omega_m$ . It also tests the gravitational instability hypothesis and the assumed biasing scheme. A successful model for the peculiar velocity field may be used to recover the distribution of galaxies or clusters in real space, directly from their measured redshift. This, in turn, allows investigation of the statistical properties of the objects’ distribution, free from the effects of redshift space distortions. Overall, model velocity fields constructed using different surveys have proved to be remarkably consistent with one another (Baker *et al.* 1998) and have been successful in reproducing most of the characteristics exhibited by maps made directly from observed peculiar velocities. There are, however, two major exceptions: the large bulk motion on very large scales claimed by Lauer and Postman (1994) and a prominent feature in the Mark III catalogue of peculiar velocities compiled by Willick *et al.* (1997) at distances larger than  $30 h^{-1} \text{ Mpc}$ , consisting of a strong shear in the Hydra-Centaurus region (Davis, Nusser and Willick 1996).

Here we present a new nonparametric model for the cosmic velocity field based on the recently completed PSCz survey of IRAS galaxies. This is the last of the near all-sky redshift surveys based on the IRAS catalogue and supersedes both the 1.2Jy and the QDOT catalogues which it contains. The denser sampling and lower flux limit of the PSCz survey allows one to model the peculiar velocity field to large scales without excessive shot noise.

The outline of this paper is as follows. In §2 we describe the PSCz dataset as well as two other redshift catalogues

<sup>\*</sup> Throughout this paper we write Hubble’s constant as  $H_0 = 100h \text{ km s}^{-1} \text{ Mpc}^{-1}$

that we use to construct independent model velocity fields. Two methods for generating the PSC<sub>z</sub> peculiar velocity fields have been implemented in order to keep track of systematic errors. These are presented in §3, together with a detailed error analysis. A cosmographic tour is performed in §4 along with a consistency check between the two PSC<sub>z</sub> velocity models and a comparison between the PSC<sub>z</sub> and 1.2Jy model velocity fields. In §5 we take advantage of the large depth of the PSC<sub>z</sub> survey to compare the gravity field derived from it with the one derived from the distribution of Abell/ACO clusters. An estimate of the parameter  $\beta \simeq \Omega_m^{0.6}/b$ , where  $b$  is the linear bias parameter of IRAS galaxies, is obtained in §6 by comparing observed and predicted bulk velocity vectors. In §7 we discuss our results further and summarize our main

## 2 THE DATASETS

The main dataset used in this work is the recently completed PSC<sub>z</sub> redshift survey described in detail by Saunders *et al.* (1998a). The main catalogue contains some 15,500 IRAS PSC galaxies with  $60 \mu\text{m}$  flux,  $f_{60}$ , greater than 0.6 Jy. To avoid cirrus contamination only PSC objects with  $f_{100} < 4f_{60}$  were selected. Stars were excluded by requiring that  $f_{60} > 0.5f_{25}$ . For our purposes, one of the most important properties of the PSC<sub>z</sub> catalogue is its large sky coverage. The only excluded regions are two thin strips in ecliptic longitude that were not observed by the IRAS satellite, the area in the galactic plane where the V-band extinction exceeds 1.5 magnitudes, and a few small isolated spots on the celestial sphere. Overall, the PSC<sub>z</sub> catalogue covers  $\sim 84\%$  of the sky. Although we will occasionally consider galaxies with recession velocity as large as  $30000 \text{ km s}^{-1}$ , for the most part we will use the PSC<sub>z</sub> subsample within  $20000 \text{ km s}^{-1}$ , containing 11206 objects. The distribution on the sky of PSC<sub>z</sub> galaxies is shown in galactic coordinates (Aitoff projection) in the upper part of Fig. 1.

For comparison purposes, we have also applied our analysis to the similar, but shallower, IRAS 1.2Jy redshift survey (Fisher *et al.* 1995a). Galaxies in this catalogue were selected from the same IRAS PSC but using a higher (ADDscan) flux limit,  $f_{60} > 1.2$  Jy, and different criteria for minimizing contamination by galactic cirrus. This catalogue has a somewhat larger sky coverage of  $\sim 88\%$ . Here we will use the 4939 IRAS 1.2 Jy galaxies within  $20000 \text{ km s}^{-1}$  of the Local Group.

Finally, in an attempt to extend our analysis, we use a completely different set of mass tracers consisting of a volume-limited sample of optically-selected galaxy clusters extracted from the Abell (1958) and the Abell, Corwin & Olowin (1989; hereafter ACO) catalogues. These were cross-calibrated according to the prescription described by Branchini and Plionis (1996; hereafter BP96). The sample has a limiting depth of  $250 h^{-1} \text{ Mpc}$  and contains 493 clusters of richness class  $R \geq 0$  at  $|b| \geq 13^\circ$ , and  $m_{10} < 17$ , where  $m_{10}$  is the magnitude of the tenth brightest galaxy in the cluster.

The number of galaxies in a flux limited sample decreases with distance, as may be seen in Fig. 2 for the PSC<sub>z</sub> (upper histogram) and 1.2 Jy (lower, shaded histogram) surveys. We define a selection function,  $\phi(r)$ , as the fraction of galaxies that can be seen out to a redshift distance  $r = \frac{cz}{H_0}$  (expressed in  $h^{-1} \text{ Mpc}$ ). To determine  $\phi(r)$  we use the parametric maximum likelihood estimate proposed by Yahil *et al.* (1991), in which the following analytic form for the selection function is assumed:

$$\phi(r) = Ar^{-2\alpha} \left( \frac{1+r^2}{r_*^2} \right)^{-\beta} \quad \text{if } r > r_s. \quad (1)$$

The value of the normalization constant  $A$  does not affect the modeling of peculiar velocities. In this work we arbitrarily set  $\phi(r) = 1$  if  $r \leq r_s$  with  $r_s = 6 h^{-1} \text{ Mpc}$ . This choice is equivalent to imposing a lower cutoff in the  $60 \mu\text{m}$  luminosity which in turns avoid giving too much weight to faint, nearby IRAS galaxies that do not reliably trace the galaxy distribution in the nearby regions (Rowan Robinson *et. al.* 1990). The relevant parameters have been determined via likelihood analysis using only the objects within  $100 h^{-1} \text{ Mpc}$ . The results are displayed in Table 1 for the PSC<sub>z</sub> and 1.2Jy surveys, both in redshift (z-) and real (R-) space (i.e. after correction for redshift space distortions as discussed in §3.1). The predicted number density of galaxies as a function of redshift distance,

predicted by eqn. (1), is shown in Fig. 2, superimposed on the observed  $N$  vs.  $r$  histograms. The theoretical curves provide a good description of the data.

Our estimator for the selection function is independent of clustering but requires a prior knowledge of the evolutionary rate. Springel and White (1998) have recently developed a new technique to estimate the rate of evolution of selection function. Their application to the the 1.2Jy catalog shows a rather strong evolution which becomes even more dramatic when applied to the PSCz catalog (Springel 1998). Ignoring such an effect would potentially cause spurious streaming motions in the model velocity. However, as we have verified, our selection function for PSCz turns out to be very similar to the one obtained by Springel (1998) within the scales relevant for our analysis. The difference between the two selection functions increases with the distance but only up to a 5 % level at  $200 h^{-1}$  Mpc. Although strong, evolutionary effects become important only beyond these scales and therefore we will neglect them when modeling the PSCz velocity field.

For the Abell/ACO composite sample we adopt the selection function derived by BP96:

$$\phi(r) = \begin{cases} 1 & \text{if } r \leq r_{c1} \\ 0.5(1 + A_1 \exp(-r/r_{\circ 1})) & \text{if } r_{c1} < r \leq r_{c2} \\ 0.5(A_2 \exp(-r/r_{\circ 2}) + A_1 \exp(-r/r_{\circ 1})) & \text{if } r > r_{c2} \end{cases} \quad (2)$$

The estimated values of the parameters are listed in Table 2, and the expected number of clusters as a function of redshift distance is shown in Fig. 2 as a thick line.

The mean separation,  $l$ , of the objects in a population of tracers limits the intrinsic resolution with which we can probe the underlying cosmic fields. A natural smoothing length,  $R_s = l$ , has therefore to be used to reflect the sparse sampling and correct for shot noise errors. In a magnitude limited survey,  $l$  increases with distance  $r$  according to:

$$l(r) = \left[ \frac{\phi(r)}{\langle n \rangle} \right]^{-1/3}, \quad (3)$$

where the average number density of objects  $\langle n \rangle$  has been estimated as

$$\langle n \rangle = \frac{1}{V} \sum_{i=1}^{N_g} \phi(r_i)^{-1}, \quad (4)$$

where the sum extends to all the  $N_g$  objects contained within the sampled volume  $V$ . The values of the mean galaxy separation at  $100 h^{-1}$  Mpc have been reported in Table 1 both for the PSCz and 1.2Jy samples. Fig. 3 shows the mean inter-object separation as a function of  $r$  for the three samples considered. Because of the shallower depth of the 1.2Jy sample, its inter-galaxy separation increases much more steeply with distance than in the PSCz sample. Thus, at a fixed resolution, the PSCz survey probes cosmic structures at larger distances than the 1.2 Jy survey without an increase in the shot noise uncertainty. The dot-dashed line in Fig. 3 shows the Abell/ACO mean intercluster separation. Locally, this is much larger than the corresponding separation for the galaxy surveys, but on scales greater than  $170 h^{-1}$  Mpc, clusters start to become more effective than IRAS 1.2Jy galaxies in tracing the cosmic density fields.

### 3 NON-PARAMETRIC MODELS OF THE COSMIC VELOCITY FIELD

The main aim of this paper is to obtain a self-consistent, non-parametric model of the velocity field in the local universe (i.e. for  $r < 150 h^{-1}$  Mpc). We do this by removing the redshift space distortions that affect the radial galaxy distribution in the survey using two different procedures. The first is the iterative technique pioneered by Strauss & Davis (1988), applied by Yahil *et al.* (1991), and further refined by Sigad *et al.* (1997). Most of the results presented here were obtained using this technique. The second procedure, used here primarily to check for possible systematic effects, is the non-iterative technique introduced by Nusser and Davis (1994).

### 3.1 The methods

The two procedures that we have implemented rely on three important assumptions. Firstly, we assume that cosmic structures have grown by the gravitational amplification of small amplitude fluctuations present in the density field at early times (gravitational instability, c.f. Peebles 1980). Secondly, we assume that fluctuations on the scales of interest are small enough that linear (or mildly non-linear) theory is applicable. Thirdly, we assume that luminous objects (galaxies or clusters) trace the underlying mass density field according to:

$$\delta_l(\mathbf{r}) = b_l \delta(\mathbf{r}), \quad (5)$$

where  $\delta$  is the mass overdensity at position  $\mathbf{r}$ ,  $\delta_l$  is the fluctuation in the number of luminous objects at this same location, and  $b_l$  is the biasing parameter. Eqn. (5) is often referred to as the “linear biasing model.”

The reconstruction methods return a model of the cosmic velocity field that depends on the parameter  $\beta = \Omega_m^{0.6}/b_l$ . The value of  $\beta$  must be determined *a posteriori* by comparison with other observational data. The two reconstruction techniques that we use have been extensively discussed and tested by Branchini *et al.* (1998) where the reader may find further details. Here, we simply outline the main points of each method.

#### Method 1: The iterative technique

In linear theory the overdensity is related to the peculiar velocity field by

$$\nabla \cdot \mathbf{v} \propto -\beta \delta_l. \quad (6)$$

The model velocity field is then obtained by iteratively solving the system of equations:

$$\mathbf{v}(\mathbf{r}) = \frac{H_0 \beta}{4\pi} \int d^3 \mathbf{r}' \frac{\mathbf{r}' - \mathbf{r}}{|\mathbf{r}' - \mathbf{r}|^3} \delta(\mathbf{r}') \quad (7)$$

and

$$\mathbf{r} = cz - \hat{\mathbf{r}} \cdot (\mathbf{v} - \mathbf{v}_{LG}). \quad (8)$$

Eqn (7) follows from integrating eqn (6);  $\mathbf{v}$  is the peculiar velocity of a tracer object at position given by the radial unit vector  $\hat{\mathbf{r}}$ ; and  $\mathbf{v}_{LG}$  is the velocity of the Local Group.

During each iteration, the selection function and the mean number density of the population of displaced objects are recomputed. Eqns (6) and (7) are only valid in the linear regime and so the force field needs to be smoothed so as to eliminate nonlinear effects. We adopt a “top hat” filter with a smoothing radius  $R_s(r) = \max[5, \frac{\langle n \rangle}{\phi(r)}]^{-1/3} h^{-1} \text{Mpc}$ . This choice eliminates most of the nonlinear contributions and keeps the shot noise at a constant level. To improve numerical convergence we adiabatically increase the value of  $\beta$  at each of ten iterations, from 0.1 to 1.0 (Strauss *et al.* 1992). The resulting model velocity field does not depend on the input value of  $\beta$  since, to first order, the amplitude of the velocity vectors scales linearly with  $\beta$ . In spite of the smoothing applied some nonlinear effects may remain. For example, around high density regions, such as clusters, there may be triple-valued regions in which the same redshift is observed at three different positions along a given line-of-sight. We correct for this by collapsing the galaxies within clusters and implementing their “robust procedure” (their “method 2”) to handle galaxy positioning inside triple-valued regions. For the collapsing procedure, we have used two different datasets: the six nearest clusters listed in Table 2 of Yahil *et al.* (1991) and a larger catalog of 61 objects obtained by merging the 59 SMAC clusters by Hudson *et al.* (1998) with the Yahil *et al.* (1991) dataset. The results show that the collapsing procedure only affect the infall pattern around rich clusters. However, at the level of smoothing used in this work the effect is negligible and no systematic differences are found when the model velocity fields are compared on a point-by-point basis.

#### Method 2: Spherical harmonics expansion

This procedure is based on the method proposed by Nusser and Davis (1994). In linear theory, the velocity field in redshift space is irrotational and thus may be derived from a velocity potential:

$$\mathbf{v}(\mathbf{s}) = -\nabla \Phi(\mathbf{s}). \quad (9)$$

Therefore, if one expands the potential and the galaxy density field,  $\delta^g$ , in spherical harmonics, and uses the Zel'dovich approximation, then the two fields obey a Poisson-like equation:

$$\frac{1}{s^2} \frac{d}{ds} \left( s^2 \frac{d\Phi_{lm}}{ds} \right) - \frac{1}{1+\beta} \frac{l(l+1)\Phi_{lm}}{s^2} = \frac{\beta}{1+\beta} \left( \delta_{lm}^g - \frac{1}{s} \frac{d \ln \phi}{d \ln s} \frac{d\Phi_{lm}}{ds} \right), \quad (10)$$

where  $\delta_{lm}^g$  and  $\Phi_{lm}$  are the spherical harmonic coefficients of the galaxy density and velocity potential fields respectively. We adopt a Gaussian filter with a smoothing radius  $R_s(r) = \max[3.2, \frac{\langle n \rangle}{\phi(r)}]^{-1/3} h^{-1} \text{Mpc}$ , compute the coefficients  $\delta_{lm}^g$  in redshift shells for the different catalogues, solve eqn. (10) for  $\Phi_{lm}$ , and then compute the full three-dimensional velocity field in redshift space using eqn. (9). Galaxy positions and peculiar velocities at the real space positions,  $\mathbf{r}$ , are obtained by assuming a one-to-one mapping between  $\mathbf{r}$  and  $\mathbf{s}$  along the line-of-sight. We minimize the problem of triple-valued regions by adopting the same cluster-collapsing scheme used above.

Redshift space distortions are only one of several effects that hamper the recovery of cosmic density and velocity fields from observational data. Incomplete sky coverage is another, potentially serious, problem and we deal with it using a filling technique similar to that introduced by Yahil *et al.* (1991). Masked regions close to the galactic plane are filled by a random cloning procedure, while masked regions at large galactic latitudes are filled with a random distribution of synthetic galaxies having the observed number density. Tests performed by Branchini *et al.* (1998) using the mock catalogs described in the next section showed that this filling technique does not introduce significant biases in the reconstructed velocities. As a further check we have also used the new Fourier Interpolation technique developed by Saunders *et al.* (1998b). In this second case we have used a radially dependent PSCz mask, which allows us to deal better with the well known PSCz incompleteness at large distance and low latitudes. The predicted velocities, however, turned out to be almost identical to the ones obtained using the random cloning technique, showing the adequacy of our original filling procedure.

Another source of random and systematic error is the radial selection function which, when coupled to redshift distortions, generates the so called 'rocket effect' discussed by Kaiser and Lahav (1989). This is a spurious acceleration measured from a magnitude-limited sample of galaxies by an observer who has a peculiar velocity unrelated to the true gravitational acceleration. In Method 1 this effect is quantified and corrected for using the mock catalogues discussed below. In Method 2 the rocket effect is explicitly accounted for by the second term in the right hand side of eqn. (10).

Finally, IRAS galaxies are preferentially of late morphological type and tend to avoid rich environments like galaxy clusters. Baker *et al.* (1998) have shown that the ratio of the amplitudes of the IRAS and optical density fields, smoothed on scales  $\geq 5 h^{-1} \text{Mpc}$ , is almost constant, implying a ratio of linear biasing parameters of  $b_o/b_I \simeq 1.4$ .

### 3.2 Error estimates using mock catalogues

We have used a suite of large cosmological N-body simulations to generate mock galaxy catalogues that mimic the main properties of the PSCz and 1.2Jy redshift surveys. We use these to quantify random and systematic errors in our reconstructed velocity fields. For the fields inferred from cluster catalogues, we adopt the error estimates derived by BP96 and by Branchini *et al.* (1997) on the basis of a hybrid Monte Carlo/mock catalogue technique.

The simulations used to generate the mock PSCz and 1.2Jy catalogues are those described by Cole *et al.* (1998). We consider two different cold dark matter cosmologies: a flat model with  $\Omega = 0.3$  and cosmological constant term,  $\Lambda c^2/3H_0^2 = 0.7$ , and a critical density universe ( $\Omega = 1.0$ ) with power spectrum shape parameter,  $\Gamma = 0.25$ . In both cases, the fluctuation amplitude was normalized by the observed abundance of galaxy clusters. This requires setting  $\sigma_8 = 0.55\Omega_m^{-0.6}$  (Eke, Cole & Frenk 1996), where  $\sigma_8$  is the linear rms mass density fluctuation in top hat spheres of radius  $8h^{-1} \text{Mpc}$ . Galaxies were identified with random particles from the simulations (so that  $b = 1$  by construction). Prior to generating the mock catalogues, we smoothed the velocities in the simulations using a top hat filter of radius  $1.5 h^{-1} \text{Mpc}$ . This brings  $\sigma_{12}(1)$ , the pairwise velocity dispersion of objects whose projected separation is  $\leq 1 h^{-1} \text{Mpc}$ , down to  $\sim 250 \text{ km s}^{-1}$  (when only particles within  $30 h^{-1} \text{Mpc}$  from the observer are considered). This value is in accordance with the recent analysis of the Optical Redshift Survey of Santiago *et al* (1995, 1996)

by Strauss, Cen and Ostriker (1998) for galaxies outside high density regions. A similar agreement is found with  $\sigma_{12}(1)$  estimated using only late type galaxies in the Perseus–Pisces redshift catalogue (Guzzo *et al.* 1997). Both these observations refer to ‘field’ galaxies, and therefore compare well with the late type IRAS galaxies of the PSCz catalog. Each mock PSCz catalog is contained in a sphere of radius  $170 h^{-1}$  Mpc, and, for the purpose of the error analyses, 10 nearly independent mock catalogs have been obtained for each cosmological model.

Several constraints were applied to the mock catalogues in order to obtain mass distributions and velocity fields as similar as possible to those observed:

- 1) Local Group observers. Hypothetical observers were selected from particles that have a velocity,  $\mathbf{v}_{LG} = 625 \pm 25$   $\text{km s}^{-1}$ , and lie in regions in which the shear within  $5 h^{-1}$  Mpc is smaller than  $200 \text{ km s}^{-1}$  and the fractional overdensity within the same scale ranges between -0.2 and 1.0 (Brown and Peebles 1987). These constraints mimic the Local Group environment.
- 2) Coherent galaxy dipole. A galactic coordinate system,  $(l, b)$ , in the (periodic) computational volume was defined such that the velocity of the observer pointed towards  $(l, b) = (276, 30)$ , the direction of the dipole anisotropy observed in the cosmic microwave background (CMB) radiation. This dipole is known to be approximately aligned with the dipole in the distribution of IRAS galaxies (Strauss *et al.* 1991, Schmoldt *et al.* 1998).
- 3) Radial selection. We generated flux-limited “galaxy” samples using a Monte Carlo rejection procedure to select particles in the simulations, assigning them fluxes according to eqn. (1). In the vicinity of an observer, the particle number density in the simulation is less than the number density of galaxies in the PSCz and 1.2Jy catalogues. We were therefore forced to generate catalogues that are semi-volume limited at a radius of  $10.9 h^{-1}$  Mpc for the PSCz and  $7.8 h^{-1}$  Mpc for the 1.2Jy cases.
- 4) Masked areas. To mimic the incomplete sky coverage, we excluded all objects within the unobserved regions in the two IRAS catalogues.

The distribution on the sky of the galaxies in one of our PSCz mock catalogues is shown, as an Aitoff projection, in the lower panel of Fig. 1, where it may be compared to the real survey displayed in the upper panel. An illustration of the utility of these mock surveys is provided in Fig. 4. The left-hand panel displays density and velocity fields projected onto the mock Supergalactic plane, after smoothing with a Gaussian filter of radius  $6 h^{-1}$  Mpc. The right-hand panel shows density and velocity fields reconstructed using Method 1 above. All the main features, as well as most of the small scales structures, are correctly reproduced. Not surprisingly, the main differences occur around  $\text{SGY} = 0$ , i.e. within the zone-of-avoidance, and close to density peaks. (Very similar results are obtained with Method 2 above.)

A complete description of the mock catalogues, their use for error estimation and a detailed assessment of the reliability of our reconstruction methods is given in Branchini *et al.* (1998) for the PSCz and 1.2Jy catalogues. The corresponding analysis for the Abell/ACO cluster catalogues may be found in Branchini *et al.* (1997).

#### 4 A COSMOGRAPHIC TOUR

In this Section we present a qualitative description of the model density and velocity fields of the local universe derived from the PSCz survey. We analyse the data using Method 1 above. Visualizing three dimensional structures and the corresponding vector fields, is not easy. Fortunately from this point of view, the most interesting structures in the nearby universe, on scales larger than the Local Supercluster are roughly distributed in a planar structure, de Vaucouleur’s (1948) Supergalactic plane (at supergalactic coordinates  $\text{SGZ} = 0$ ). In this analysis we will mainly follow the somewhat traditional way of displaying the density and velocity features by projecting onto this plane. However distribution of structures onto planes parallel to the Supergalactic one is discussed as well.

The depth and sampling frequency of the PSCz dataset allows a reliable map of the density field to be constructed within a sphere around us of radius  $150 h^{-1}$  Mpc. Fig. 5 shows the adaptively smoothed overdensity field within this sphere, projected onto the Supergalactic plane. Within  $30 h^{-1}$  Mpc a constant Gaussian filter of radius  $3 h^{-1}$  Mpc has been used to smooth the field, but beyond that the radius of the filter increases linearly with distance

up to  $11.25h^{-1}$  Mpc at  $150h^{-1}$  Mpc. This smoothing maintains a roughly constant sampling error within the volume. The  $\delta = 0$  level is indicated by the yellow line. The most striking feature of this map is the large scale coherence of the mass distribution. Interconnected overdensities, separated by very large voids, extend over distances of order of  $100h^{-1}$  Mpc. The most prominent structure, which plays a major role in the dynamics of the local flow field, is the overdense ridge that extends from the Perseus–Pisces supercluster, close to the centre of the map, all the way to the Shapley concentration near the top left corner.

The PSCz survey is large enough to allow the velocity field corresponding to the mass distribution to be reconstructed fairly accurately, with a relative error always smaller than 50 % in the region depicted in figure 5. This precision, however, is higher than that with which peculiar velocities can be measured at those distances and so we cannot compare our model predictions with velocity data over the entire region of Fig. 5. Such a comparison can only be carried out reliably over a smaller volume of radius  $\sim 80h^{-1}$  Mpc. For this reason we now describe in some detail our reconstructions within this distance.

#### 4.1 The PSCz model density and velocity fields within $80h^{-1}$ Mpc

Fig. 6 shows the PSCz model density and velocity fields smoothed with a  $6h^{-1}$  Mpc Gaussian and projected onto the Supergalactic plane. Overdensity contours, both positive (continuous lines) and negative (dashed lines), are drawn in steps of  $\Delta\delta = 0.5$ . The  $\delta = 0$  contour is represented by a thick, continuous line. The amplitude of the velocity vectors is on an arbitrary scale.

With a  $6h^{-1}$  Mpc smoothing, the Local Supercluster, centered on the Virgo cluster at  $(\text{SGX}, \text{SGY}) = (-2.5, 11.5)$ , does not appear as an isolated structure but is connected instead to the prominent Hydra–Centaurus supercluster at  $(\text{SGX}, \text{SGY}) = (-35, 20)$ . Together with the Pavo–Indus–Telescopium supercluster [ $(\text{SGX}, \text{SGY}) = (-40, -15)$ ], the latter makes up the well known Great Attractor. The Coma cluster and its neighbour, A1367, appear as a peak at  $(\text{SGX}, \text{SGY}) = (0, 75)$ , slightly elongated in the SGX direction. The Perseus–Pisces supercluster is clearly visible at  $(\text{SGX}, \text{SGY}) = (45, -20)$  and is the second largest peak on the map, well separated from its northern extension [ $(\text{SGX}, \text{SGY}) = (45, 20)$ ] which is sometimes called the Camelopardalis supercluster. Finally, the Cetus Wall may be seen as an elongated structure around  $(\text{SGX}, \text{SGY}) = (15, -50)$ . The Sculptor void [ $(\text{SGX}, \text{SGY}) = (-20, -45)$ ] is the largest underdensity in the map, but is almost matched in size by a void in the background of the Camelopardalis supercluster. Three more underdense regions that exert an important influence on the local dynamics are the voids in the foreground of Coma [ $(\text{SGX}, \text{SGY}) = (-10, 50)$ ], in the background of the Perseus–Pisces complex [ $(\text{SGX}, \text{SGY}) = (50, -50)$ ], and behind the Great Attractor [ $(\text{SGX}, \text{SGY}) = (-60, 10)$ ].

The competing dynamical roles of the various overdense and underdense structures seen in Fig 6. determine the local velocity field in a complex manner that cannot be simply described as a bulk flow or a multi-spherical infall model. The local velocity field implied by the PSCz density field is illustrated by the vectors plotted in Fig. 6. Its dominant features are the large infall patterns towards the Great Attractor, Perseus–Pisces and Coma. A striking feature is the large-scale coherence of the velocity field, apparent as a long ridge between Cetus and Perseus–Pisces and as a large-scale flow along the Camelopardalis, Virgo, Great Attractor baseline and beyond (see §5). A prediction of the PSCz data is the lack of prominent back-infall onto the Great Attractor region. The flow around it appears to be determined by the compressional push of two voids (at  $(\text{SGX}, \text{SGY}) = (-10, 50)$  and  $(-60, 10)$ ) and the pull of the Shapley Concentration on much larger scales (see §5). These features are present also when Method 2 is used for the reconstruction (§4.2), or when the 1.2Jy survey is used as the input catalogue (§4.3). As pointed out by Davis, Nusser & Willick (1996), this model velocity field does not match the Mark III peculiar velocity field (Willick *et al.* 1997a) which exhibits a large outflow away from the Centaurus supercluster and an inflow onto the Hydra complex. Also, there is no evidence for a motion of the Perseus Pisces supercluster towards us.

Fig. 7 extends our qualitative analysis to two planes of constant SGZ,  $40h^{-1}$  Mpc above and below the Supergalactic plane. At  $\text{SGZ} = +40h^{-1}$  Mpc the density field (Fig 7b) is dominated by a large void which is connected to the Local Void identified by Tully (1987). The prominent peak at  $(\text{SGX}, \text{SGY}) = (40, -40)$  seems to be an extension of the Perseus–Pisces supercluster. The relative velocity field (Fig 7a) is still characterized by a coherent, large-

scale, flow towards the same direction  $[(\text{SGX}, \text{SGY}) = (-50, 50)]$  as the stream seen in the Supergalactic plane. At negative  $\text{SGZ} = -40 h^{-1} \text{ Mpc}$  the extensions of the Pavo–Indus–Telescopium  $(-50, 15)$  and Perseus–Pisces  $(20, -20)$  superclusters are visible. The dynamical effect of these two peaks is evident in the associated large infall patterns (Fig. 7c).

#### 4.2 Comparison of the two reconstruction methods

A detailed quantitative analysis based on mock PSC $z$  catalogs have been performed by Branchini *et al.* (1998) to evaluate random errors, also showed that the predicted velocity field is not affected by significant systematic bias. To further check this result we have compared the reconstructions produced by the two different methods discussed in §3.1. Figs. 8a and 8b show the predicted velocity fields smoothed with a  $6h^{-1} \text{ Mpc}$  Gaussian and projected onto the Supergalactic plane. The two methods succeed in reproducing the main features that we have already highlighted: remarkable large-scale coherence in the velocity field, clear infall patterns onto Coma, Perseus–Pisces and the Great Attractor but no back-infall onto the latter. The only noticeable difference is that Method 2 seems to blur slightly the sharp features (like the Cetus ridge) produced by Method 1 in the velocity field.

Quantitative evidence for the similarity of the two model fields is provided in Fig 8c, which shows a scatterplot of the SGX Cartesian components of the reconstructed velocity fields measured within  $80h^{-1} \text{ Mpc}$  at gridpoints with  $\text{SGZ} = 0$ . The peculiar velocities in the two models should obey the linear equation,

$$M_2 = BM_1 + A, \quad (11)$$

where  $M_1$  and  $M_2$  denote any of the Cartesian components of the peculiar velocity predicted by Methods 1 and 2, respectively and  $B$  is expected to be 1 if no systematic errors are present. The offset  $A$  allows for possible differences in the predicted bulk flows in the two models. We obtain the values of  $A$  and  $B$  by minimizing

$$\chi^2 = \sum_{i=1}^{N_t} \frac{(M_{2,i} - A - BM_{1,i})^2}{(\sigma_{M_1,i}^2 + B^2 \sigma_{M_2,i}^2)}, \quad (12)$$

where  $\sigma_{M_1,i}$  and  $\sigma_{M_2,i}$  are the errors in the velocities at a generic gridpoint  $i$  in the two methods, and  $N_t$  is the total number of points used for the comparison. We assume that  $\sigma_{M_1,i} = \sigma_{M_2,i} \equiv \sigma$ , so that Eqn. 12 becomes

$$\chi^2 = \frac{1}{\sigma^2} \sum_{i=1}^{N_t} \frac{(M_{2,i} - A - BM_{1,i})^2}{(1 + B^2)} = \frac{\chi_o^2}{\sigma^2}. \quad (13)$$

Only  $N_i$  of the  $N_t$  points used in the comparison are independent. It can be shown that the quantity  $\chi_{eff}^2 = (N_i/N_t)\chi^2$  is approximately distributed as  $\chi^2$  with  $N_{d.o.f} = N_i - 2$  degrees of freedom (e.g. Hudson *et al.* 1995). We can therefore approximately evaluate  $\sigma$  by setting  $\chi_{eff}^2 = N_{d.o.f}$  so that

$$\sigma^2 = \frac{\chi_o^2 N_i}{N_t(N_i - 2)}. \quad (14)$$

We take  $N_i$  to be the number of independent volumes within the volume sampled,  $N_i \simeq 7.5$ , taking into account the smoothing filter. We then find a regression slope,  $B = 1.04 \pm 0.06$ , and a negligible zeropoint,  $A = 3 \pm 2$ , indicating that there are no systematic differences between the two peculiar velocity fields produced by Methods 1 and 2. The dispersion around the fit for the SGX Cartesian component of the peculiar velocities turns out to be  $\sigma_v = 48 \beta \text{ km s}^{-1}$  in both two methods. This represents the intrinsic error in the reconstruction procedure and is nearly a factor 2 smaller than the average total error obtained from the error analysis on the mock PSC $z$  catalogues (which also account for uncertainties in the filling procedures, nonlinearity, finite volume etc.). Similar results are obtained for the SGZ component and even better agreement is found for the SGY component for which the uncertainties in the filling procedure of the zone-of-avoidance are less important.

### 4.3 Comparison of the PSCz and 1.2Jy model velocity fields

Because they were drawn from the same parent catalogue, we expect the PSCz and 1.2Jy catalogues to give consistent model velocity fields, at least in the nearby volume where the sampling by 1.2Jy galaxies is not too sparse. In analogy with the PSCz fields displayed in Fig. 6, Fig. 9 shows the 1.2Jy density and velocity fields, smoothed with a  $6h^{-1}$  Mpc Gaussian, and projected onto the Supergalactic plane. Most of the characteristic structures identified in Fig. 6 are also visible in Fig. 9 except that underdense regions in the 1.2Jy map appear somewhat more extended than in the PSCz map. The overall pattern in the PSCz velocity field is reproduced in the 1.2Jy map although the large-scale coherent flow along the Camelopardalis, Great Attractor baseline is less evident in the 1.2Jy map. On the other hand, the infall pattern around the Great Attractor in the 1.2Jy survey spreads out over a larger region. These discrepancies might well be due to the larger shot noise uncertainties in the 1.2Jy catalog.

Our 1.2Jy model velocity field is consistent with that derived independently by Webster, Lahav and Fisher (1997) using the method developed by Fisher *et al.* (1995b). Comparison with their Fig. 7d (which assumes a CDM model with  $\Gamma = 0.2$  as a prior in the Wiener filtering technique) reveals only one noticeable difference between the two maps. This is in the region of the Great Attractor, where the model of Webster *et al.* predicts a weak back-infall. The discrepancy, however, is small and may simply reflect our use of a constant  $6h^{-1}$  Mpc Gaussian smoothing, which is somewhat larger than the smoothing applied by Webster *et al.* .

Fig. 10b shows a comparison between the PSCz and 1.2Jy overdensity fields, both smoothed with  $6h^{-1}$  Mpc Gaussian and tabulated onto  $64^3$  grids. Only those gridpoints lying along the Supergalactic plane and within  $80 h^{-1}$  Mpc of the Local Group position are considered. As in the previous section we fit a straight line to the data and estimate the parameters by minimizing  $\chi^2$ . The slope of this line is close to unity, indicating that there are no detectable systematic differences between the reconstructions based on the PSCz and 1.2Jy catalogues. The scatter is  $\sigma_\Delta = 0.12$ , and it is likely that most of it is due to shot noise in the 1.2Jy field. Similar considerations apply to the velocity–velocity comparison in Fig 10a in which, as in Fig 8c, we only show the SGX Cartesian component of the velocity. There is a non–negligible zeropoint offset of  $120\beta \text{ km s}^{-1}$  in the SGX components of the cumulative bulk flow in the two models. However, this difference is comparable to the  $1-\sigma$  uncertainty in the reconstruction of each Cartesian component of the bulk velocity (see §6.1 below). The peculiar features in the velocity–velocity scatterplot reflect correlated velocities within individual cosmic structures. For example, the elongated structure running parallel to the best–fit line corresponds to the infall pattern onto the Perseus–Pisces supercluster which appears to be somewhat more prominent in the 1.2 Jy reconstruction.

## 5 MODELLING VERY LARGE SCALE MOTIONS

The sampling density of the PSCz survey is high enough to allow an investigation of the density field out to  $\sim 120 h^{-1}$  Mpc even with a  $6h^{-1}$  Mpc Gaussian smoothing. This is illustrated in Fig. 11 which displays the usual density and velocity model fields projected onto the Supergalactic plane. The shot noise in this map is still tolerable, at a level comparable to that in the maps discussed in §4.1. The larger volume mapped now reveals the full extent of the coherent streaming involving galaxies from the Camelopardalis Supercluster all the way to the Shapley Concentration (that begins to appear at  $(\text{SGX}, \text{SGY}) = (-100, +60)$ ), passing through the Local Supercluster and the Great Attractor.

The dynamical sources of the coherent motion seen in Fig. 11 are the same ones that we identified earlier as those responsible for the flow pattern behind the Great Attractor. The gravitational pull is mostly due to the Shapley Concentration while the coherence is aided by the joint push of the two large voids (at  $(\text{SGX}, \text{SGY}) = (-80, 10)$  and  $(\text{SGX}, \text{SGY}) = (-50, 70)$ ) that were only partially visible in Fig. 6. The map also reveals a large extension to other underdense regions, the Sculptor void and the two connected voids behind the Cetus–Perseus–Pisces–Camelopardalis complex.

In Fig. 12 we show the density field projected onto four planes parallel to the Supergalactic one, placed at  $\text{SGZ} = \pm 40$  and  $\text{SGZ} = \pm 80$ . Fig. 13 shows the related velocity field. The same structures that we have identified in Fig. 7 can be now traced over larger scales while keeping the shot noise error at a low level so that we can

fully appreciate the large scale coherence of the features both in the density and the velocity field. For example, in Fig. 12a the void originally identified in Fig. 7b, appears to extend over a much larger region, also along the SGZ axis (Fig. 13a and 13b). Similarly, the stream towards  $(\text{SGX}, \text{SGY}) = (-50, 50)$  that we have identified in the planes at  $\text{SGZ} = 0$  and  $\text{SGZ} = +40 \text{ } h^{-1} \text{ Mpc}$  it is also present at  $\text{SGZ} = +80 \text{ } h^{-1} \text{ Mpc}$ . No very large scale features are identified on the plane at  $\text{SGZ} = -40 \text{ } h^{-1} \text{ Mpc}$  (Fig. 12c and 13c) which, as we have previously noticed, is dominated by a few infall patterns associated to the southern extensions of Pavo–Indus–Telescopium and Perseus–Pisces superclusters. Coherent structures in the density field and the related streaming motions are can be identified on the plane at  $\text{SGZ} = -80 \text{ } h^{-1} \text{ Mpc}$ .

### 5.1 Comparison with the Abell/ACO model fields

Different surveys of IRAS and optical galaxies have been used to construct various model velocity fields which proved to be remarkably consistent (Yahil *et al.* 1991, Kaiser *et al.* 1991, Hudson 1994, Baker *et al.*, 1998). We repeat a similar exercise using a completely different set of mass tracers, the Abell/ACO clusters, to model the density and velocity fields up to very large scales, although with much larger sampling errors. BP96 have already employed the Abell/ACO cluster subsample described §2 to model the density and velocity fields up to scales of  $250 \text{ } h^{-1} \text{ Mpc}$ . The reconstruction technique they used is a simplified version of our Method 1 (cf. §3.1) in which the selection function (which is nearly constant on the scales of interest) is not iteratively updated and no special treatment is given to triple-valued regions. In order to compare the PSC $z$  and cluster model fields we smooth both using a Gaussian of width  $20 \text{ } h^{-1} \text{ Mpc}$ . Such a large smoothing is required because of the large intercluster separation.

Fig. 14 shows the smoothed density fields projected onto the Supergalactic plane within a distance of  $150h^{-1} \text{ Mpc}$ , as derived from the PSC $z$  (upper panel) and cluster (lower panel) catalogues. Overdensity contours are plotted in steps of  $\Delta\delta = 0.2$ , for the galaxy field, and of  $\Delta\delta = 0.88$  for cluster field. This is equivalent in rescaling the cluster field by a factor  $b_c = 4.4$  which is the relative linear biasing parameter inferred in §5.2 below. As before the heavy line traces the  $\delta = 0$  contour. The dashed lines show the approximate location of the zone-of-avoidance in the PSC $z$  ( $|b| \leq 8^\circ$ ) and cluster ( $|b| \leq 20^\circ$ ) samples.

Despite of the  $b_c = 4.4$  rescaling, which has been introduced to account for the relative bias between the two population of objects, the density peaks appear more prominent in the cluster sample than in the PSC $z$  map. This may reflect greater undersampling by IRAS galaxies of the cores of rich clusters than was indicated by Baker *et al.* (1998), or it may be due to shot noise in the cluster sample which, in spite of the heavy smoothing applied, is still substantial. It should be noted, however, that both the Great Attractor region  $(\text{SGX}, \text{SGY}) = (-50, 0)$  and the Perseus–Pisces supercluster  $(\text{SGX}, \text{SGY}) = (50, -20)$  where the effect is strongest, both lie within the zone-of-avoidance of the cluster sample. It is therefore possible that the height of these peaks has been artificially amplified by the coupling between shot noise and the filling-in procedure. (For this reason we shall exclude the region at  $|b| \leq 20^\circ$  from the quantitative analysis in §5.2 below.) Above  $|b| = 20^\circ$  the Shapley Concentration  $(\text{SGX}, \text{SGY}) = (-120, 70)$  is the only peak with a larger amplitude in the cluster map than in the PSC $z$  map. This comparison could be affected by the fact that beyond  $60h^{-1} \text{ Mpc}$  we do not perform a cluster–collapsing procedure in Method 1 and so it is possible that the reconstruction method may be placing PSC $z$  galaxies at incorrect positions within clusters in the Shapley concentration. Amplitudes aside, the positions of the peaks in the two density maps are very similar. The low density regions are also approximately coincident, although they are less extended in the cluster map in which voids also appear somewhat shallower. The latter effect simply reflects the fact that the assumption of local biasing,  $\delta_c = b_c \delta_g$ , breaks down at low  $\delta_g$  because of the constraint  $\delta_c \geq -1$ .

Fig. 15 shows the velocity fields inferred from the two samples, again at a  $20h^{-1} \text{ Mpc}$  smoothing and projected onto the Supergalactic plane. The amplitude of the velocity vectors is on an arbitrary scale but, in the clusters case, the velocity vectors have been rescaled by  $b_c = 4.4$ . The two large overdensities lying within the zone-of-avoidance in Fig. 15b largely determine the infall patterns at those locations  $[(\text{SGX}, \text{SGY}) = (-50, 0)]$  and  $[(\text{SGX}, \text{SGY}) = (50, -20)]$ . Beyond  $|b| = 20^\circ$ , however, the galaxy and cluster velocity fields show remarkable similarity. Both exhibit a large coherent flow along the Camelopardalis, Great Attractor, Shapley Concentration baseline. The infall onto the

Shapley region is more prominent in the cluster map, but, in general, the velocity field patterns are very similar at positive SGY, with an outflow at positive SGX, and a convergent flow towards the Shapley Concentration at negative SGX. Below the zone-of-avoidance (negative SGY) both maps show outflow from the Sculptor void, but this is less prominent in the clusters case.

## 5.2 The relative linear bias between galaxy cluster and IRAS galaxies.

If biasing is a local process (see e.g. Cole *et al.* 1998) then, in the regime where mass fluctuations are small, we expect the level of the bias to be independent of scale. This expectation is consistent with the results of POTENT analyses performed by Dekel *et al.* (1993) and Sigad *et al.* (1997) and we expect it to be valid in the present analysis in which the PSCz and cluster density and velocity fields have been smoothed with a  $20h^{-1}$  Mpc filter. Thus, on the scales of interest, we expect the two model density and velocity fields to be linearly related:

$$C = Pb_c + A_c, \quad (15)$$

where  $C$  and  $P$  stand for cluster and PSCz and represent either  $\delta$  or any one of the Cartesian components of the velocity field. The constant  $b_c$  is the bias parameter of clusters relative to IRAS galaxies and  $A_c$  allows for a relative offset in the mean density or bulk velocities of the two fields. For quantitative analyses it is most convenient to use the SGY Cartesian component of the velocity field since this is the least affected by uncertainties in filling in the zone-of-avoidance. To estimate  $b_c$  we adopt the strategy of Hudson *et al.* (1995) and Branchini *et al.* (1997), already used in §4.2, of regressing the two model fields by minimising the quantity

$$\chi^2 = \sum_{i=1}^{N_t} \frac{(C_i - A_c - b_c P_i)^2}{(\sigma_{C,i}^2 + b_c^2 \sigma_{P,i}^2)}, \quad (16)$$

where the subscript  $i$  refers to any of the  $N_t$  gridpoints within the comparison volume. The quantities  $\sigma_{C,i}$  and  $\sigma_{P,i}$  represent the errors in the cluster and PSCz fields, respectively.

The errors in the cluster field,  $\sigma_{C,i}$ , have been estimated by Branchini *et al.* (1997). They are the sum in quadrature of the intrinsic errors in the reconstruction procedure, as estimated by BP96 using Montecarlo techniques, and the shot noise uncertainties (which, for the very sparse cluster fields dominate), evaluated using the mock catalogue generated by Kolatt *et al.* (1996) which is designed to reproduce the distribution of structures in our local universe. A typical error in the cluster overdensity field is  $\langle \sigma_{C,\delta} \rangle = 0.36$ , while for the SGY-component of the velocity field it is  $\langle \sigma_{C,v_y} \rangle = 250\beta \text{ km s}^{-1}$ .

The errors in the PSCz fields have been estimated using the mock catalogues described in §3.2. The basic procedure consists of comparing the density and velocity fields obtained by applying Method 1 to the mock galaxy catalogues with the true fields in the parent N-body simulation. We have characterized the reconstruction errors by noticing that the residuals correlate with distance, galactic latitude and, for the velocity field, with the signal itself. From the analysis of the mock catalogues, we have derived two approximate expressions for the errors (valid for  $|b| > 20^\circ$ ):

$$\langle \sigma_{P,\delta} \rangle = 0.11 - 6.7 \cdot 10^{-4} \cdot b + 3.3 \cdot 10^{-4} \cdot r \quad (17)$$

and

$$\langle \sigma_{P,v_y} \rangle = 70 + 2.7 \cdot 10^{-1} \cdot r + 0.15 \cdot |v_y|, \quad (18)$$

where  $r$  is the distance measured in  $h^{-1}$  Mpc,  $b$  is the galactic latitude in degrees, and  $|v_y|$  is the amplitude of the SGY Cartesian component in  $\text{km s}^{-1}$ . The actual assumed error at a gridpoint has been generated from a Gaussian distribution centred on  $\langle \sigma_P \rangle$  with dispersions of 0.04 for the overdensity and  $40 \text{ km s}^{-1}$  for the  $v_y$  field, respectively.

The regression of the PSCz and cluster fields uses all the gridpoints within  $120 h^{-1}$  Mpc and outside the cluster zone-of-avoidance (i.e. at  $|b| > 20^\circ$ ). As a result of the large smoothing applied not all the gridpoints in the comparison volume are independent. The number of independent points,  $N_i$ , can be computed as in Dekel *et al.* (1993),

$$N_i^{-1} = N_t^{-2} \sum_{j=1}^{N_t} \sum_{i=1}^{N_t} \exp(-r_{ij}^2/2R_s^2), \quad (19)$$

where  $r_{ij}$  is the separation between gridpoints  $i$  and  $j$  and  $R_s$  is the smoothing radius of the Gaussian filter. As in §4.2 we define the  $\chi_{\text{eff}}^2 \equiv (N_i/N_t)\chi^2$  statistics which correspond, in practice, to multiplying the errors  $\sigma_P$  and  $\sigma_C$  by  $\sqrt{N_t/N_i}$  in equation (16). We use this statistic to assess the errors on  $b_c$  and  $A_c$ .

Fig. 16a shows a  $\delta$ - $\delta$  scatterplot of the model cluster and PSCz overdensity fields measured at  $\sim 1000$  randomly selected gridpoints. All 6426 original points are used in the regression analysis. The solid line shows the best fit obtained by minimizing  $\chi_{\text{eff}}^2$  and the parameters of the fit are listed in Table 3. The resulting bias parameter is  $b_c^\delta = 4.4 \pm 0.6$ . This is compatible with results from independent analyses (e.g. Peacock and Dodds 1994). The parameter  $S^\delta = \chi_{\text{eff}}^2/N_{\text{dof}}$  is close to 1, which may be taken as an indication that the errors have not been grossly over- or underestimated. The systematic difference in the amplitude of the density peaks in the cluster and IRAS  $\delta$  fields, noticed in Fig 14a, manifests itself as a deviation from the best fitting line at large  $\delta_{\text{PSCz}}$ . Restricting the regression to values of  $\delta_{\text{PSCz}} \leq 0.35$  has a small impact on the final result, returning  $b_c^\delta = 4.5 \pm 0.6$ , almost identical to the previous value, and  $S^\delta = \chi_{\text{eff}}^2/N_{\text{dof}} = 1.15$ . This suggests that the exact weighting of PSCz galaxies in high density regions has only a minor effect on the regression analysis, mainly because the overdensity mismatch in large density peaks is restricted to a very few gridpoints. As a further check, we have repeated the  $\delta$ - $\delta$  regression using a PSCz velocity model derived without applying our standard procedures for collapsing clusters and handling triple valued regions (which should exacerbate any discrepancies associated with high peaks.) The results, listed in the second row of Table 3, show that the effect on  $b_c$  is indeed very small, leading to  $b_c^\delta = 4.5 \pm 0.6$ .

Fig. 16b displays the scatterplot of the SGY Cartesian component of the two velocity fields in which, as in fig. 16a we only show  $\sim 1000$  randomly selected gridpoints to avoid overcrowding. As shown in Table 3 the slope of the best fitting line is  $b_c^{v_y} = 4.7 \pm 0.6$  and no significant zeropoint offset is detected, indicating that the SGY components of the cluster and PSCz bulk flows are consistent with one another over the scales of interest. However, as indicated in Table 3., the resulting  $\chi_{\text{eff}}^2$  is large, resulting in a  $S^{v_y} = 1.55$ . This could be the result of underestimating the errors. Indeed, the error analysis by Branchini et al. (1997) uses clusters from the Kolatt et al. (1996) mock catalogs that do not accurately match the Abell/ACO cluster distribution and velocities. We can obtain  $S^{v_y} \simeq 1.0$  if we allow by a very reasonable error underestimate in the cluster field of  $\sim 30\%$ , in which case we would obtain  $b_c^{v_y} = 4.0 \pm 0.6$ . Note that a  $1\sigma$  agreement between  $b_c^\delta$  and  $b_c^{v_y}$  is obtained whether or not the cluster errors have been effectively underestimated.

It is worth emphasizing that the agreement of the  $\delta$ - $\delta$  and  $v_y$ - $v_y$  comparisons is not trivial. The  $\delta$ - $\delta$  comparison is local; it is hardly affected by problems related to filling in masked regions but is potentially prone to the cluster core weighting problem. The  $v_y$ - $v_y$  comparison, on the other hand, involves the distribution of objects within the entire sample and thus is much more strongly affected by the unknown mass distribution within the zone-of-avoidance and beyond the sample's edge. We might therefore expect the two comparisons to be affected by different biases. The agreement in the estimate of  $b_c$  from the two analyses suggests that systematic biases have been properly taken into account and that the linear biasing assumption is a good approximation, at least on scales larger than our  $20 h^{-1}$  Mpc smoothing.

## 6 THE BULK VELOCITY VECTOR

In this section we consider the peculiar velocity,  $\mathbf{v}_b(R)$ , of spheres of radius  $R$  centred on the Local Group. This is a low order statistic that can readily be estimated observationally and which has a theoretical counterpart. The expectation value of the bulk velocity,  $|\mathbf{v}_b|$ , averaged over scale  $R$  is:

$$\langle |\mathbf{v}_b(R)|^2 \rangle = \frac{\beta^2}{2\pi^2} \int P(k) W(kR)^2 dk, \quad (20)$$

where  $P(k)$  is the power spectrum of density fluctuations.  $W(kR) = 3 \frac{\sin(kR) - kR \cos(kR)}{(kR)^3}$  is the Fourier transform of the spherical top hat window function in real space which is chosen to allow a straightforward comparison between the

theoretical definition (eq. 20) and its observational analogous (eq. 21). If the initial fluctuation field obeys Gaussian statistics, then evolution through gravitational instability preserves a Gaussian distribution for the amplitude of each Cartesian components of  $\mathbf{v}_b(R)$ , so that  $|\mathbf{v}_b(R)|$  has a Maxwellian distribution. This property makes it difficult to constrain  $P(k)$  from the measured  $\mathbf{v}_b(R)$ . Nevertheless, comparison of the measured  $\mathbf{v}_b(R)$  with the velocities predicted from the PSCz gravity field allows, in principle, an estimate of the  $\beta$  parameter. In practice, however, the bulk velocity is extremely sensitive to systematic errors both in the observational data and in the models. We attempt to take this carefully into account in the following analysis.

### 6.1 The model bulk flow

The basis for our treatment of random and systematic errors in the bulk velocity vector are, again, the mock PSCz catalogues described in §3.2. From each mock catalogue we generate a model velocity field using Methods 1 and 2 of §3.2. The field is then smoothed onto a  $64^3$  cubic grid of side  $192 h^{-1}$  Mpc using a  $12h^{-1}$  Mpc Gaussian filter. Such a large smoothing is chosen in order to obtain an error estimate appropriate to the homogeneous, quantitative comparisons with the Mark III and SFI bulk velocity data that we will perform in §6.2. We measure the cumulative bulk velocity vector in the CMB frame by averaging over the peculiar velocities measured at gridpoints:

$$\mathbf{v}_b(R) = \frac{\sum_{(i,j,k) < R} \mathbf{v}_{i,j,k}}{\sum_{(i,j,k) < R}}, \quad (21)$$

where  $\mathbf{v}_{i,j,k}$  is the predicted velocity vector in the CMB frame at gridpoint  $(i, j, k)$ . The sum  $\sum_{(i,j,k) < R}$  extends over all the gridpoints contained within a sphere of radius  $R$ . The same exercise is then repeated using the original N-body velocity field. This gives an unbiased estimate of the true bulk velocity in the mock catalogue and the comparison between the true and reconstructed bulk velocities provides an estimate of the error in the reconstruction.

The filled circles in Fig. 17a show the mean difference between the amplitude of the cumulative bulk flow reconstructed using Method 1 and the true bulk flow, averaged over the different mock catalogues and measured at different radii. The mean value indicates the systematic error in the reconstruction while the errorbars, which give the variance around the mean, measure the random uncertainty. Very similar results are obtained if the reconstruction is carried out using Method 2. Note that the random errors decrease with distance (from  $\sim 80 \text{ km s}^{-1}$  at  $10 h^{-1}$  Mpc to  $\sim 50 \text{ km s}^{-1}$  at  $100 h^{-1}$  Mpc), while the systematic errors increase with distance and become comparable to the random noise at large radii. Systematic errors come mainly from two sources: the filling-in procedure for the zone-of-avoidance and the modelling of the Local Group velocity. Since our two reconstruction methods work in the Local Group frame, the predicted Local Group velocity vector, obtained from the dipole of the galaxy distribution, must be added to the model velocities. As a result, errors in the determination of the dipole (arising, for example, from shot noise, finite volume and the rocket effect) affect the model bulk velocity vector. The uncertainties due to the filling-in procedure may be minimized by restricting attention to the SGY component of the bulk velocity. As shown by the open symbols in Fig. 17a the improvement is quite dramatic, reducing the systematic error to  $< 20 \text{ km s}^{-1}$ .

The errors displayed in Fig. 17a cannot readily be used to make quantitative corrections to the PSCz model bulk flow since their amplitude depends on  $\beta$ , the only free parameter in the model velocities. However, we can take advantage of the fact that, to first approximation, the model velocities scale linearly with  $\beta$ . Thus, the ratio between the reconstructed and true bulk velocities should be independent of  $\beta$ . This ratio, averaged over our mock catalogues, is shown by filled circles in Fig. 17b, as a function of distance, with errorbars representing the relative variance. Since it is independent of  $\beta$ , this ratio may be used as a multiplicative factor to correct the predicted PSCz bulk flow amplitudes for systematic errors. As expected, the corrections become very small when considering the SGY component (open circles). We have performed a similar analysis to estimate errors in the PSCz bulk velocity obtained using Method 2 and in the 1.2Jy bulk flow model, obtained using Method 1.

We are now ready to estimate PSCz and 1.2Jy model bulk flows and their uncertainties. Fig 18a shows the amplitude of the cumulative bulk velocity vector, predicted using various methods and redshift surveys. The velocities are normalized to  $\beta = 1$ . Open and filled circles show PSCz results using Methods 1 and 2 respectively, and filled

squares show results from the 1.2Jy survey, all corrected for systematic errors as discussed in the preceding paragraph. For clarity only the  $1-\sigma$  error bars from Method 1 are plotted. The filled triangles show the bulk velocity computed from the Abell/ACO model velocity field, rescaled by  $b_c = 4.4$  (see §5.2). There is remarkably good agreement between the cumulative bulk flows computed from the different sets of mass tracers, with typical deviations of less than  $\sim 20\%$  from the mean in the amplitude from the different surveys and analysis methods. The directions of the cumulative bulk flow vectors, measured within  $60 h^{-1} \text{ Mpc}$ , are plotted in Fig. 18b. The PSC $z$  model bulk flow points within  $1\sigma$ , with the direction of both the 1.2Jy and Abell/ACO model bulk flows. The direction of the CMB dipole, indicated by the asterisk, is plotted for reference at the centre of the figure.

So far we have modelled bulk velocities in the nearby universe by considering only the effect of the mass distribution within  $200h^{-1} \text{ Mpc}$ , as traced by IRAS galaxies or Abell/ACO clusters. Bulk flows, however, are sensitive to the mass distribution on scales larger than those probed by our samples. We can correct for this missing large-scale contribution in a statistical fashion, assuming linear theory and using eqn. (20). The correction factor is the ratio

$$F(P(k), k_{min}) = \frac{\int_0^\infty P(k)W(kR)^2 dk}{\int_{k_{min}}^\infty P(k)W(kR)^2 dk}. \quad (22)$$

The numerator in this equation is the mean true bulk flow, while the denominator is the mean bulk flow generated only by density fluctuations on scales smaller than  $R_{max} = \frac{2\pi}{k_{min}}$ . In our case,  $R_{max} \sim 200h^{-1} \text{ Mpc}$ . Note that the ratio depends only on the spectral shape and on  $k_{min}$ , while the dependency on  $\beta$  has cancelled out. Since the bulk flow obeys a Maxwellian distribution, we can estimate the uncertainty in this correction and add it in quadrature to the error in our estimate of the bulk flow calculated from the mock catalogues. In computing  $F$  we assume a CDM model with spectral shape  $\Gamma = 0.25$ , as indicated by a wide variety of data on the large-scale galaxy distribution (e.g. Baugh 1996)

We have applied the correction of eqn. (22) to the PSC $z$  bulk velocity reconstructed using Method 1. The resulting cumulative bulk velocity (for  $\beta = 1$ ) is shown in Fig. 18a as a dot-dashed line labelled M1L. We regard this as our best estimate of the  $\beta$ -dependent bulk flow.

## 6.2 Model vs. observed bulk flow

In this Section, we compare our best estimate of the predicted bulk flow velocity from the PSC $z$  survey with recent observational estimates. Such a comparison serves two purposes. Firstly, consistency between predicted and observed velocities lends support to the hypothesis that structure grew by gravitational instability and gives confidence in the integrity of the observational data. Secondly, the comparison allows an estimate of the parameter  $\beta = \Omega_0^{0.6}/b$ .

The determination of bulk flows from peculiar velocity surveys is prone to systematic errors. For example, zero-point errors in the calibration of the distance indicators coupled with limited sky coverage may mimic a bulk flow. Similarly, the coupling of large intrinsic errors in distance measurements with inhomogeneities in the density distribution (the inhomogeneous Malmquist bias) also results in a spurious outflow. Thus to perform an unbiased comparison with theoretical predictions requires full-sky, homogeneous surveys of peculiar velocities and an accurate model of the survey's window function.

In Fig. 19 we plot observational determinations of bulk flows derived from four (almost) independent datasets. The black triangles (taken from Strauss 1997) represent the cumulative bulk flow in the Mark III catalogue (Dekel 1997). The sparse and noisy Mark III velocities have been smoothed assuming that the velocity field is irrotational. This guarantees that a unique three-dimensional velocity field is derivable from the observed radial velocities, as in the POTENT method (Dekel, Bertschinger & Faber 1990). The resulting three-dimensional peculiar velocity field, smoothed with a  $12h^{-1} \text{ Mpc}$  Gaussian, and defined on a regular grid is directly comparable to our model prediction. The black square shows the estimate by da Costa *et al.* (1996) of the bulk velocity on a scale of  $60 h^{-1} \text{ Mpc}$ , derived from the SFI catalogue of peculiar velocities (Giovanelli *et al.* 1997a, 1997b), using a POTENT-smoothing technique similar to the one applied to the Mark III data. The grey triangle is the bulk velocity inferred from 44 supernovae Type Ia by Riess, Press & Kirshner (1995), as reported by Dekel (1997). The effective radius of this last measurement

is much smaller than the depth of the sample because the data were weighted by the inverse of the errors. Finally, the grey square at large distance shows the bulk velocity derived by Lauer & Postman (1994; LP94) from a sample of brightest cluster galaxies. The directions of the observed bulk velocity vectors are given in Fig. 19b. For the Mark III and supernovae estimates, they have been estimated from data within  $50 h^{-1}$  Mpc, and for the SFI from data within  $60 h^{-1}$  Mpc. The direction of the LP94 bulk flow is taken from Strauss (1997) and refers to a depth of  $\sim 90 h^{-1}$  Mpc.

Except for the LP94 result, there is excellent agreement between the various determinations of the bulk flow in Fig. 19. These may be compared with the bulk flows predicted by the PSCz survey, indicated by the thick dot-dashed lines which enclose the  $1-\sigma$  allowed range. The lower panel shows the cumulative bulk flow as a function of distance, normalized to  $\beta = 0.76$  while the upper panel shows its SGY component only, this time normalized to  $\beta = 0.55$ . The filled circle in Fig. 19b marks the direction of the model bulk velocity vector within  $50 h^{-1}$  Mpc.

Requiring that the amplitude of the predicted bulk flow should match the directly measured value gives an estimate of  $\beta$ . In obtaining this estimate we shall ignore the discrepant LP94 result which Strauss *et al.* (1995) and Watkins and Feldman (1995), amongst others, have argued is inconsistent with currently acceptable cosmological models. The same considerations applies for our model bulk flow which only relies on the gravitational instability and linear biasing hypotheses. As shown in Fig. 19, matching the amplitude of the LP94 bulk flow would require a value of  $\beta = 1.87$ , which is not only incompatible with all the current measurements (e.g. Table 1 in Dekel 1997) but also does not help in reducing the very large misalignment of  $70^\circ$  between the two vectors.

Recent analyses of existing peculiar velocity catalogues show some inconsistencies in the calibration of distance indicators which may result in spurious bulk flow signals (Willick and Strauss 1998). For this reason we limit our comparison of model and observed bulk flows by imposing a series of restrictions designed to minimize possible systematic errors. This should return an unbiased, if somewhat less accurate, estimate of  $\beta$ . These restrictions are:

- We consider only Mark III and SFI bulk velocities which, like the PSCz model velocity field, have been smoothed onto a regular grid and filtered on a similar scale. This ensures that the comparison is as homogeneous as possible.
- We exclude scales below  $20 h^{-1}$  Mpc since small differences in the smoothing procedures applied to model and observed velocities in the the nearby region can bias the comparison.
- We do not consider Mark III velocities at distances greater than  $30 h^{-1}$  Mpc because beyond this distance, doubts have been expressed about the integrity of the Mark III data by Davis, Nusser & Willick (1996) and by Willick & Strauss (1998). At smaller distances, on the other hand, there is no evidence for any systematic effects in the Mark III data and, furthermore, the bulk flow inferred from them agrees well with that inferred from the SFI data, as shown in Fig. 19.

From these considerations, the most reliable estimate of  $\beta$  is obtained by comparing the amplitude of the Mark III cumulative bulk flow at  $30 h^{-1}$  Mpc ( $440 \pm 45 \text{ km s}^{-1}$ ) with the PSCz model bulk velocity returned by Method 1 at this same distance ( $(576 \pm 84)\beta \text{ km s}^{-1}$ ). This gives  $\beta = 0.76 \pm 0.13$ , where the errors are  $1-\sigma$ . Performing the comparison between the model and SFI bulk velocities at  $60 h^{-1}$  Mpc gives a consistent result,  $\beta = 0.67 \pm 0.16$ . This consistency is reassuring because the SFI data, unlike the Mark III data, show no systematic differences with the 1.2Jy gravity field (da Costa *et al.* 1996). These  $\beta$  estimates have been obtained after correcting for systematic errors in the predicted buck flow that we have obtained from the PSCz mock catalogs. As shown above, systematic uncertainties in the model bulk flows are greatly reduced when we consider its SGY component which is the least affected by the zone-of-avoidance. To minimise the uncertainties associated to this empirical correction we compare the SGY components of the Mark III cumulative bulk flow ( $110 \pm 40 \text{ km s}^{-1}$ ) with the PSCz model bulk velocity ( $(202 \pm 49)\beta \text{ km s}^{-1}$ ) at  $30 h^{-1}$  Mpc. This returns a value of  $\beta = 0.55 \pm 0.25$  ( $\beta = 0.54 \pm 0.28$  if the SFI bulk velocity is compared instead) which, given the large uncertainties, is still consistent with the one previously obtained at  $1-\sigma$  level.

## 7 DISCUSSION AND CONCLUSIONS

The recently completed PSCz redshift survey of IRAS galaxies represents an almost ideal dataset for studying the mass distribution and the gravity field in the local universe. In this paper we have used the PSCz survey to develop

a nonparametric model of the local cosmic velocity field which supersedes results derived from the shallower 1.2 Jy and the sparser QDOT surveys. Our reconstructions are based on the assumptions that cosmic structure has grown by gravitational instability and that fluctuations in the galaxy distribution are proportional to fluctuations in the mass distribution. We have paid particular attention to a careful estimation of random and systematic errors using a suite of mock PSC $z$  catalogues constructed from large cosmological N-body simulations. As a further check on the validity of our results, we have implemented two independent methods for reconstructing the PSC $z$  model velocity fields, both of which give consistent results.

Because of the large size of the PSC $z$  survey, the density and velocity fields can be reliably reconstructed out to a depth of  $150h^{-1}$  Mpc. We have presented maps of the galaxy distribution which, with a smoothing of only  $6h^{-1}$  Mpc, clearly show the relative sizes of the main structures that characterize our local universe. The two largest peaks in our neighbourhood are the Great Attractor, made up of the Hydra–Centaurus and Pavo–Indus–Telescopium superclusters, and the Perseus–Pisces supercluster located in roughly the opposite direction on the Supergalactic plane. The Local, Coma-A1367, and Camelopardalis superclusters as well as the Cetus Wall are clearly visible in our maps, and the giant Shapley concentration appears near the edge of the survey, behind the Great Attractor. The largest underdensity in our vicinity is the well-known Sculptor void, but this is almost matched in size by a void in the background of the Camelopardalis supercluster. Three more underdense regions that exert an important influence on the local dynamics are the voids in the foreground of Coma, in the background of the Perseus–Pisces complex, and behind the Great Attractor.

The local velocity field implied by the PSC $z$  density field is complex. The dominant features are the large infall patterns towards large mass concentrations in the Great Attractor, Perseus–Pisces and Coma regions. Superimposed upon these are impressive coherent flows along a ridge between Cetus and Perseus–Pisces and along the Camelopardalis–Virgo–Great Attractor–Shapley direction. We see no prominent back-infall onto the Great Attractor. Instead, the flow is in this region results from the interplay between the compressional push of two nearby voids and the pull of the Shapley Concentration on much larger scales.

The PSC $z$  reconstruction agrees well with results from the 1.2Jy survey within  $80h^{-1}$  Mpc, the region in which the latter provides adequate sampling. The only noticeable difference are the predicted bulk velocity vectors (in the CMB frame) which differ in the two surveys by  $\sim 130\beta$  km s $^{-1}$  in each Cartesian component. This discrepancy arises from uncertainties in the way in which the zone-of-avoidance is filled in and from errors in the transformation of the predicted peculiar velocities from the Local Group to the CMB frame. While the former affect the PSC $z$  and 1.2Jy results equally, the latter are more severe in the 1.2Jy case because of the larger shot noise. Thus, the misalignment between the Local Group acceleration and the CMB dipole vectors is  $\sim 25^\circ$  for the 1.2Jy survey compared with only  $\sim 15^\circ$  in the PSC $z$  survey (Schmoldt *et al.* 1998). Comparison of the spherical harmonic multipoles of the two model velocity fields in radial shells confirms the consistency of the PSC $z$  and 1.2Jy survey predictions in the region of overlap (Teodoro *et al.* 1998).

As was the case with the 1.2Jy survey, the velocity field reconstructed from the PSC $z$  survey is partly inconsistent with the peculiar velocities in the Mark III catalogue. A visual inspection of the two velocity maps (Figs. 6 and 9) shows a significant difference around the Hydra–Centaurus complex, where the Mark III data exhibit a large shear, and in the Perseus Pisces region, which, in the Mark III catalog, appears to be to be part of a large streaming motion (Davis, Nusser and Willick 1996). As pointed out by Davis, Nusser & Willick (1996), beyond  $30h^{-1}$  Mpc there is a large coherent residual dipole in the difference of the 1.2Jy gravity field and Mark III peculiar velocity field. This cannot be blamed on an improper modelling of the gravity field by IRAS galaxies since the dipole depends only on the mass within the surveyed volume. Furthermore, Baker *et al.* (1998) have shown that the gravity field in the optical ORS survey (Santiago *et al.* 1995, 1996) is consistent with the 1.2Jy gravity field (and thus, by implication, with the PSC $z$  field as well). This suggests that the undersampling of cluster cores by the predominantly spiral galaxy population in IRAS surveys does not have a large effect in the inferred gravity field. The most plausible explanation for the discrepancy between the Mark III velocities and the IRAS (and ORS) model predictions seems to be some systematic bias that affects the Mark III catalogue beyond  $30h^{-1}$  Mpc (Baker *et al.* 1998, Willick and Strauss 1998).

As we saw in §5.1, the density and velocity fields inferred from the PSCz survey agree well with those inferred from a sample of Abell/ACO clusters. This is perhaps surprising since clusters are selected in a very different way from galaxies, but it is reassuring and suggests that systematic errors are under control in both cases. Comparison of the two model density and velocity fields, smoothed on the same cubic grid, out to a distance of  $140 h^{-1}$  Mpc, gives the relative linear bias,  $b_c$ , between the rich cluster and PSCz galaxy populations. A simple  $\chi^2$  analysis of the density-density and velocity-velocity comparisons gives very similar results in both cases,  $b_c = 4.4 \pm 0.6$  and  $b_c = 4.7 \pm 0.6$ , respectively. These values are consistent with the estimate,  $b_c = 4.5$ , obtained by Peacock and Dodds (1994) from an analysis of phenomenological power spectra. A more detailed comparison of the relative bias field of clusters and galaxies will be presented in Plionis *et al.* (1998).

Finally, from the reconstructed PSCz peculiar velocity field we have estimated the bulk velocities of concentric spheres around us. Comparison of these bulk flows with independently measured peculiar velocities yields an estimate of the parameter  $\beta = \Omega^{0.6}/b$ . In order to perform a homogeneous comparison while minimizing possible biases due to the Mark III-IRAS mismatch discussed above, we restricted this comparison to the amplitude of the PSCz model and the Mark III bulk velocities at  $30 h^{-1}$  Mpc. This gave our best estimate,  $\beta = 0.76 \pm 0.13$ . A similar comparison, but using the bulk flow measured in the SFI survey at  $60 h^{-1}$  Mpc (Giovanelli *et al.* (1997a, 1997b), returned a consistent estimate of  $\beta$ . To further minimize possible biases in the predicted bulk flow we also compared the SGY components of the PSCz and the Mark III bulk flow vectors, resulting in a lower value of  $\beta = 0.55 \pm 0.25$  still consistent with the previous one within  $1-\sigma$  level. These estimates of  $\beta$  are also consistent with results from analyses of the PSCz dipole (Schmoldt *et al.* 1998, Rowan-Robinson *et al.* 1998), and with the most recent determinations of  $\beta$  from velocity-velocity comparisons (Davis, Nusser & Willick 1996, da Costa *et al.* 1996, Willick *et al.* 1997b, Strauss & Willick 1998).

A determination of  $\beta$  to 15% accuracy is possible by comparing the peculiar velocity field inferred from the PSCz survey with measured peculiar velocities at independent locations. An analysis of this kind using based on the likelihood VELMOD technique (Willick *et al.* 1997b) is currently in progress.

## ACKNOWLEDGEMENTS

EB, LT and CSF thank Michael Strauss and Marc Davis for providing us with the original version of their reconstruction codes. This work was supported by various PPARC grants and by the EC TMR network for research in “Galaxy formation and evolution.” CSF acknowledges a PPARC Senior Research Fellowship.

## REFERENCES

Abell G.O., 1958, *ApJS*, 3, 211

Abell G.O., Corwin H.G., Olowin R.P., 1989, *ApJS*, 70, 1

Babul A., Weinberg D., Dekel A., Ostriker J.P., 1994, *ApJ*, 427, 1

Baker J., Davis M., Strauss M., Lahav O., Santiago B., 1998 *astro-ph/9802713/*

Baugh, C., 1996, *MNRAS*, 280, 267

Branchini E., Plionis M., 1996, *ApJ*, 460, 569 [BP96]

Branchini, E., Plionis, M. Zehavi, I., Dekel, A., 1997, *MNRAS*, *submitted*

Branchini, E., Teodoro, L. Schmoldt, I., Frenk, C., Efstathiou, G., 1998, *in preparation*

Brown, M., Peebles P. 1987, *ApJ*, 317, 588

Cole, S., Hatton, S., Weinberg, D., and Frenk C. 1998, *astro-ph/980125*

Davis M., Peebles P.J.E., 1985, *ARA&A*, 21, 109

Davis M., Nusser, A., Willlick J. 1997, *ApJ* 473, 22

da Costa L., Freudling W., Wegner G., Giovanelli R., Haynes M., Salzer J., 1996, *ApJ*, 468, L5

Davis M., Nusser, A., Willlick J. 1997, *ApJ*, 473, 22

Dekel A., Bertschinger E., Faber S.M., 1990, *ApJ*, 364, 349

Dekel A., Bertschinger E., Yahil A., Strauss M., Davis M., Huchra J., 1993, *ApJ*, 412, 1

Dekel A., 1994, *ARA&A*, 32, 371

Dekel, A, 1997, in da Costa L.N., Renzini A., eds, *Galaxy Scaling Relations*. Springer, p. 245

de Vaucouleurs G. 1948, *Ann. d'Astrophysique*, 11, 247

Eke, V., Cole, S., and Frenk, C. 1996, *MNRAS* 282, 263

Fisher K., Huchra J.P., Strauss M., Davis M., Yahil A., Schlegel D., 1995a, *ApJS*, 100, 69.

Fisher K., Lahav O., Hoffman Y., Lynden-Bell D., Zaroubi S., 1995b, *MNRAS*, 272, 885.

Giovanelli R., Haynes M., Herter T., Vogt N., Wegner G., Salzer J., da Costa L., Freudling W., 1997a, *AJ*, 113, 22

Giovanelli R., Haynes M., Herter T., Vogt N., da Costa L., Freudling W., Salzer J., Wegner G., 1997b, *AJ*, 113, 53

Guzzo, L., Strauss, M., Fisher K., Giovanelli, R., and Haynes M. 1997, *ApJ*, 489, 37

Han M., Mould J., 1990, *ApJ*, 360, 448.

Hudson M.J., 1994, *MNRAS*, 266, 475

Hudson M., Dekel A., Courteau S., Faber S.M., Willick J.A., 1995, *MNRAS*, 274, 305

Kaiser N., and Lahav, O., 1988,

Kaiser N., Efstathiou G., Ellis R., Frenk C., Lawrence A., Rowan-Robinson M., Saunders W., 1991, *MNRAS*, 252, 1

Kolatt T., Dekel A., Ganon G., Willick J.A., 1996, *ApJ*, 458, 419

Lauer T., Postman M., 1994, *ApJ*, 425, 418 [LP94]

Lynden-Bell D., Faber S.M., Burstein D., Davies R., Dressler A., Terlevich R., Wegner G., 1988, *ApJ*, 326, 19

Nusser A., Davis M., 1994, *ApJ*, 421, 1L

Peebles P.J.E., 1980, *The Large Scale Structure of the Universe*, Princeton University Press, Princeton

Peebles P.J.E., 19988, *ApJ*. 332, 17

Plionis M., *et al.* 1998 *in preparation*

Riess A., Press W., Kirschner R., 1995, *ApJ*. 438, L17

Rowan-Robinson M., Lawrence A., Saunders W., Crawford J., Ellis R., Frenk C.S., Parry I., Xiaoyang X., Allington-Smith, J., Efstathiou G., Kaiser N., 1990, *MNRAS*, 247, 1

Santiago, B. X., Strauss, M., Lahav, O., Dressler, A., and Huchra, J., 1995, *ApJ*, 446, 457

Santiago, B. X., Strauss, M., Lahav, O., Davis, M., Dressler, A., and Huchra, J., 1996, *ApJ*, 461, 38

Saunders W. *et al.* 1998a, in Proc. of the XXXII Moriond Astrophysics Meeting. *in press*

Saunders W. *et al.* 1998b, *in preparation*

Schmoldt I., 1988, *MNRAS*, *submitted*

Shaya E., Tully B., Pierce M., 1992, *ApJ*, 391, 16

Sigad Y., Dekel A., Strauss M., Yahil A., 1998, *ApJ*, 495, 516

Springel V. 1996, *Topology and Luminosity Function of the PSCz Redshift Survey*, M.Sc. Thesis, Eberhard-Karls-Universität Tübingen

Springel V., White S.D.M. 1998, *MNRAS*, *in press*

Strauss M., Davis M., 1988, in Rubin V.C., Coyne G., eds, *Large Scale Motions in the Universe: A Vatican Study Week*. Princeton Univ. Press, Princeton, p. 255

Strauss M.A., Davis M., Yahil A., Huchra J.P., 1990, *ApJ*, 361, 49

Strauss M.A., Yahil A., Davis M., Huchra J.P., Fisher K., 1992, *ApJ*, 397, 395

Strauss M.A., Cen R.Y., Ostriker J.P., Lauer T.R., Postman M., 1995, *ApJ*, 446, 507

Strauss M.A., Willick J.A., 1995, Phys Rep., 261, 271  
Strauss, M., 1997, in N. Turok ed., Critical Dialogues in Cosmology, World Scientific, p.423.  
Strauss M.A., Ostriker, J., and Cen, R. 1998, ApJ, 493,39  
Teodoro L., *et al.* 1998 *preparation*  
Tully B., 1997, Nearby Galaxy Catalog, Cambridge University Press  
Watkins R., Feldman H., 1995, ApJ, 453, 73  
Webster M., Lahav O., Fisher K., 1997, MNRAS, 287, 425  
Willlick J., Courteau S., Faber S., Burstein D., Dekel A., Strauss M., ApJS, 1997a, 109, 333.  
Willlick, J., Strauss, M., Dekel, A., and Kolatt, T. 1997b, ApJ, 486, 629  
Willlick, J., and Strauss, M. 1998, astro-ph/9801307  
Yahil A., Strauss M.A., Davis M., Huchra J.P., 1991, ApJ, 372, 380

**Table 1.** Parameters for the selection function of IRAS Galaxies

Sample	$\alpha$	$\beta$	$r_s$	$r_\star$	$l(100)$
z-IRAS PSCz	0.54	1.83	6.0	87.00	11.67
R-IRAS PSCz	0.52	1.92	6.0	90.75	11.66
z-IRAS 1.2Jy	0.49	1.80	6.0	51.27	16.21
R-IRAS 1.2Jy	0.47	1.87	6.0	52.50	16.24

**Table 2.** Parameters for the selection function of Abell/ACO clusters

Sample	$r_{\odot 1}$	$r_{\odot 2}$	$r_{c1}$	$r_{c2}$	$A_1$	$A_2$	$\langle n \rangle$
Abell/ACO	31.8	44.0	180	235	125	289	$4.61 \cdot 10^{-5}$

**Table 3.** The cluster/IRAS galaxy relative bias parameter,  $b_c$ . The top and bottom rows give results with and without applying the cluster collapsing procedure. Column 1:  $N_t^\delta$ , the number of gridpoints used for the regression; column 2:  $N_{d.o.f.}$ , the number of independent volumes for the regression; column 3:  $b_c^\delta$  from the  $\delta$ - $\delta$  regression and its 1- $\sigma$  error; column 4:  $A_\delta$ , the zero point offset in the  $\delta$ - $\delta$  regression and its 1- $\sigma$  error; column 5:  $S^\delta = \chi_{eff.}^2/N_{dof}$  from the  $\delta$ - $\delta$  regression; column 6:  $b_c^{v_y}$  from the  $v_y$ - $v_y$  regression and its 1- $\sigma$  error; column 7:  $A_{v_y}$ , the zero point offset in the  $v_y$ - $v_y$  regression and its 1- $\sigma$  error; column 8:  $S^{v_y} = \chi_{eff.}^2/N_{dof}$  from the  $v_y$ - $v_y$  regression.

$N_t$	$N_{d.o.f.}$	$b_c^\delta$	$A^\delta$	$S^\delta$	$b_c^{v_y}$	$A^{v_y}$	$S^{v_y}$
6427	54	$4.4 \pm 0.6$	$0.06 \pm 0.07$	1.14	$4.7 \pm 0.6$	$-16 \pm 90$	1.55
6527	55	$4.5 \pm 0.6$	$0.12 \pm 0.07$	1.15	$4.6 \pm 0.6$	$8.2 \pm 91$	1.57

## FIGURE CAPTIONS

**Figure 1.** Aitoff projection of the galaxy distribution in galactic coordinates, in the PSCz survey (upper panel) and in a mock catalogue constructed from a cosmological N-body simulation (lower panel). The filled in regions show unobserved or obscured regions; the zone-of-avoidance is the quasi-horizontal strip surrounding the galactic plane.

**Figure 2.** The number of galaxies as a function of redshift distance in the PSCz (upper histogram) and 1.2 Jy (lower, shaded histogram) samples. The curves show the expected counts as a function of distance estimated from the selection functions. The heavy line at the bottom shows the predicted distance distribution of Abell/ACO clusters. The labels give the total number of objects in each sample.

**Figure 3.** Mean separation as a function of radial distance (in  $h^{-1}$  Mpc) of objects in the three samples considered in this paper: PSCz galaxies (continuous line), 1.2 Jy galaxies (dashed line) and Abell/ACO clusters (dot-dashed line).

**Figure 4.** Density and velocity fields in a mock PSCz catalogue projected onto the mock ‘‘Supergalactic’’ plane. The hypothetical observer is located in a region analogous to the Local Group. Data are shown in a sphere of  $80h^{-1}$  Mpc radius centred on the observer. Both density and velocity fields have been smoothed using a Gaussian filter of radius  $6h^{-1}$  Mpc. The plot on the left shows the true fields while the plot on the right shows the reconstructed fields using Method 1. Continuous lines represent isodensity contours with a spacing of 0.25 in  $\delta$ . Solid lines encompass overdensities and dashed lines underdensities. The heavy line indicates the  $\delta = 0$  contour level. The amplitude of the velocity vectors is on an arbitrary scale.

**Figure 5.** Real space density field derived from the PSCz survey. The field has been smoothed with a variable Gaussian filter and projected onto the Supergalactic plane. The smoothing is set at a constant scale of  $3h^{-1}$  Mpc within  $30h^{-1}$  Mpc and linearly increases with the distance up to a Gaussian of  $11.25h^{-1}$  Mpc at  $150h^{-1}$  Mpc, where the most distant structure are located. The yellow line shows the  $\delta = 0$  contour.

**Figure 6.** Real space density and velocity fields derived from the PSCz survey. The fields have been smoothed with a  $6h^{-1}$  Mpc Gaussian and projected onto the Supergalactic plane. The most distant structures are located at  $80h^{-1}$  Mpc. The thick continuous line shows the  $\delta = 0$  contour. Positive (continuous lines) and negative (dashed lines) contours are plotted at steps of  $\Delta\delta = 0.5$ . The amplitude of the velocity vectors is on an arbitrary scale. This reconstruction has been performed using Method 1.

**Figure 7.** Real space density and velocity fields derived from the PSCz survey. The fields have been smoothed with a  $6h^{-1}$  Mpc Gaussian and projected onto two slices parallel to the Supergalactic plane. Panels (a) and (b) refer to the slice at  $SGZ = +40h^{-1}$  Mpc, above the Supergalactic plane, while panels (c) and (d) refer to the slice at  $SGZ = -40h^{-1}$  Mpc, below the galactic plane. Density and velocity fields are plotted separately following the same conventions adopted in Fig. 6. This reconstruction has been performed using Method 1.

**Figure 8.** The peculiar velocity field reconstructed using Method 1 (top left panel) and Method 2 (top right panel), smoothed with a  $6h^{-1}$  Mpc Gaussian and projected onto the Supergalactic plane. The amplitude of the velocity vectors is on the same arbitrary scale in the two panels. Panel (c) is the scatterplot of the SGX components of the velocity vectors illustrated in the upper panels. Only points within  $80h^{-1}$  Mpc and with  $SGZ = 0$  have been included. The parameters of the linear fit, (A,B), are indicated in the legend along with the scatter in the model velocities, ( $\sigma$ ).

**Figure 9.** Real space density and velocity fields derived from the 1.2Jy survey. The fields have been smoothed with a  $6h^{-1}$  Mpc Gaussian and projected onto the Supergalactic plane. The overdensity levels and the amplitude of the velocity vectors are as in Fig. 6. This reconstruction has been performed using Method 1.

**Figure 10.** Comparison of the 1.2Jy and PSCz density and velocity fields. Densities and velocities are measured at the same grid positions in both cases and only points with  $SGZ = 0$  and distance  $\leq 80h^{-1}$  Mpc are included. The upper panel shows the velocity–velocity comparison using the SGX components of the peculiar velocity, while the lower panel shows the  $\delta$ – $\delta$  comparison. The parameters of the linear regression fit are indicated in both panels.

**Figure 11.** Real space density and velocity fields derived from the PSCz survey. The fields have been smoothed with a  $6h^{-1}$  Mpc Gaussian and projected onto the Supergalactic plane. This figure is similar to Fig. 6, except that it displays data in a larger spherical volume of radius  $120h^{-1}$  Mpc. The thick continuous line shows the  $\delta = 0$  contour.

Positive (continuous lines) and negative (dashed lines) contours are plotted at steps of  $\Delta\delta = 0.5$ . The amplitude of the velocity vectors is on an arbitrary scale. This reconstruction has been performed using Method 1.

**Figure 12.** Real space PSC $z$  density field derived from PSC $z$  survey smoothed with a  $6h^{-1}$  Mpc Gaussian and projected onto four slices parallel to the Supergalactic plane. Panels (a), (b), (c) and (d) refers to slices at SGZ=+40, +80, -40 and -80  $h^{-1}$  Mpc, respectively. The same conventions adopted in Fig. 7 are adopted.

**Figure 13.** PSC $z$  velocity field smoothed with a  $6h^{-1}$  Mpc Gaussian and projected onto the four slices displayed in Fig. 13.

**Figure 14** Real space density fields derived from the PSC $z$  survey (upper panel) and Abell/ACO clusters (lower panel). Both fields have been smoothed with a  $20h^{-1}$  Mpc Gaussian and projected onto the Supergalactic plane within a distance of  $140 h^{-1}$  Mpc. The  $\delta = 0$  level is indicated by the thick line. Other contours are plotted in steps of  $\Delta\delta = 0.2$  for the PSC $z$  map and  $\Delta\delta = 0.88$  for the clusters map. The dashed lines delineate the zone-of-avoidance in each sample.

**Figure 15** Peculiar velocity fields derived from the PSC $z$  survey (upper panel) and Abell/ACO clusters (lower panel). Both fields have been smoothed with a  $20h^{-1}$  Mpc Gaussian and projected onto the Supergalactic plane within a distance of  $140 h^{-1}$  Mpc. The amplitude of the velocity vectors is on an arbitrary scale, with the clusters' field normalized according to a relative bias parameter,  $b_c = 4.4$ . The dashed lines delineate the zone-of-avoidance in each sample.

**Figure 16** Density and velocity scatterplots for the reconstructions based on the PSC $z$  survey and a sample of Abell/ACO clusters. For clarity only  $\sim 1000$  out of 1878 gridpoints within a sphere of radius  $120h^{-1}$  Mpc, having  $|b| \geq 20^\circ$ , are plotted. The velocity–velocity comparison in the upper panel refers to the SGY–component of the velocity and is restricted to gridpoints in which the misalignment between the two model velocity vectors,  $\Delta\theta < 30^\circ$ . The lower panel shows the  $\delta$ – $\delta$  comparison. The parameters in the legend refer to the  $\chi^2$  fits discussed in the text (see also Table 3). The errorbars give the mean  $1-\sigma$  errors in the two model fields.

**Figure 17** Random and systematic errors in the model bulk flow derived from analysis of the mock PSC $z$  catalogues. The upper panel shows the difference between the true amplitude of the cumulative bulk flow at different radii and the values reconstructed using Method 1. The lower panel shows the ratio of these two amplitudes. In both panels the circles give mean values and the errorbars standard deviations around the mean. Filled circles refer to the total bulk velocity and open circles to its SGY–component only.

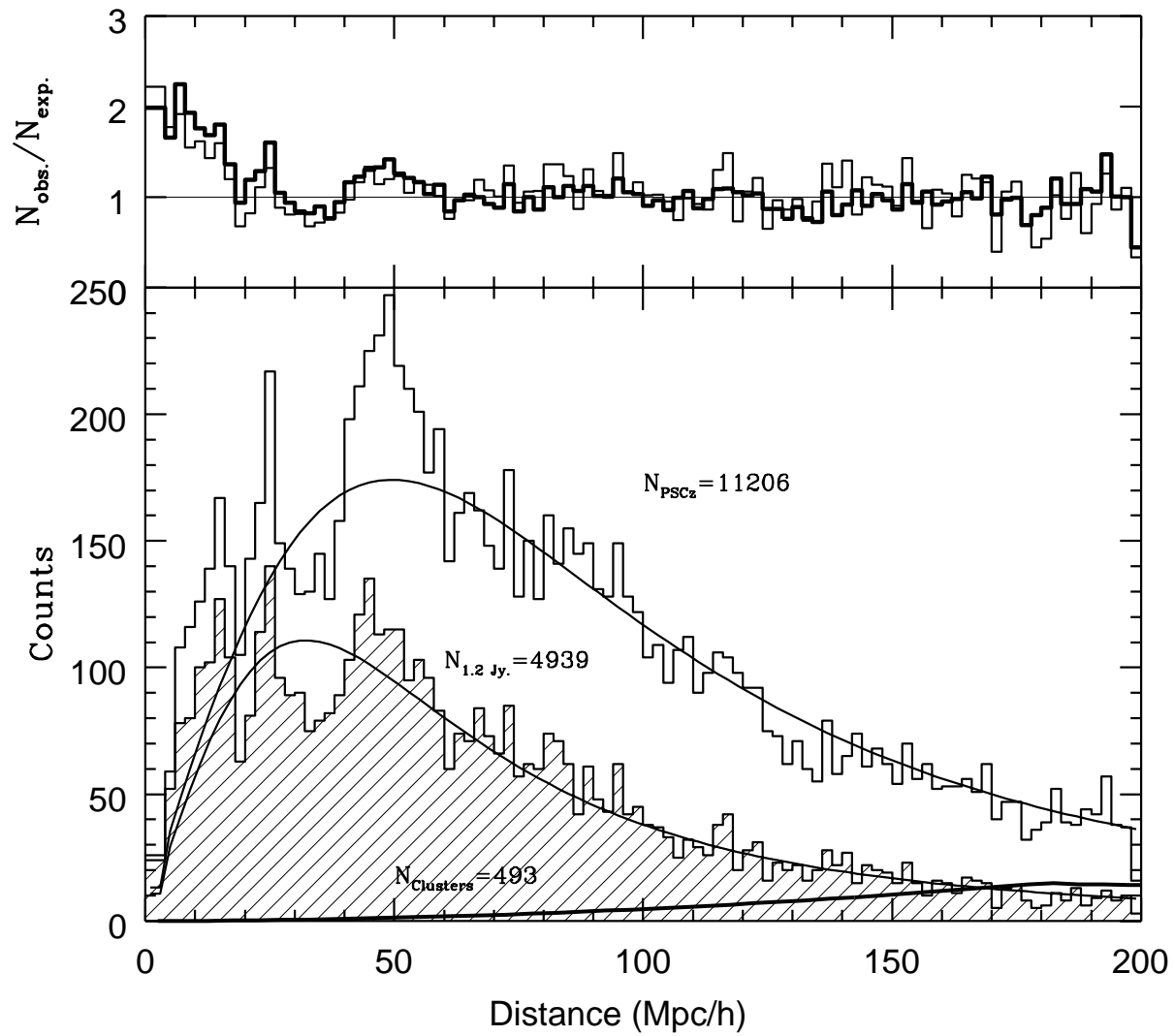
**Figure 18** The amplitude (left) and direction (right) of the cumulative bulk velocity vector predicted in different models. The circles give results from the PSC $z$  survey using Method 1 (open circles) and Method 2 (filled circles); the filled squares give results from the 1.2Jy survey; the triangles give results from the Abell/ACO cluster sample. For the models based on IRAS galaxies, the amplitudes have been normalized to  $\beta = 1$ , while for the cluster model the velocities have been normalized assuming a relative bias,  $b_c = 4.4$ . The errorbars give  $1-\sigma$  uncertainties obtained from the PSC $z$  survey using Method 1. The dot–dashed line shows the PSC $z$  reconstruction using Method 1, but including the contribution to the velocity from density fluctuations on scales larger than  $200 h^{-1}$  Mpc. The right-hand panel gives the direction of the predicted cumulative bulk flow at  $60 h^{-1}$  Mpc in galactic coordinates ( $l, b$ ). The asterisk at the centre corresponds to the direction of the CMB dipole. Errorbars are  $1-\sigma$  uncertainties derived from the analysis of the mock catalogues. The contours are set at constant misalignment angle from the apex of the CMB dipole, in steps of  $\Delta\theta = 10^\circ$ .

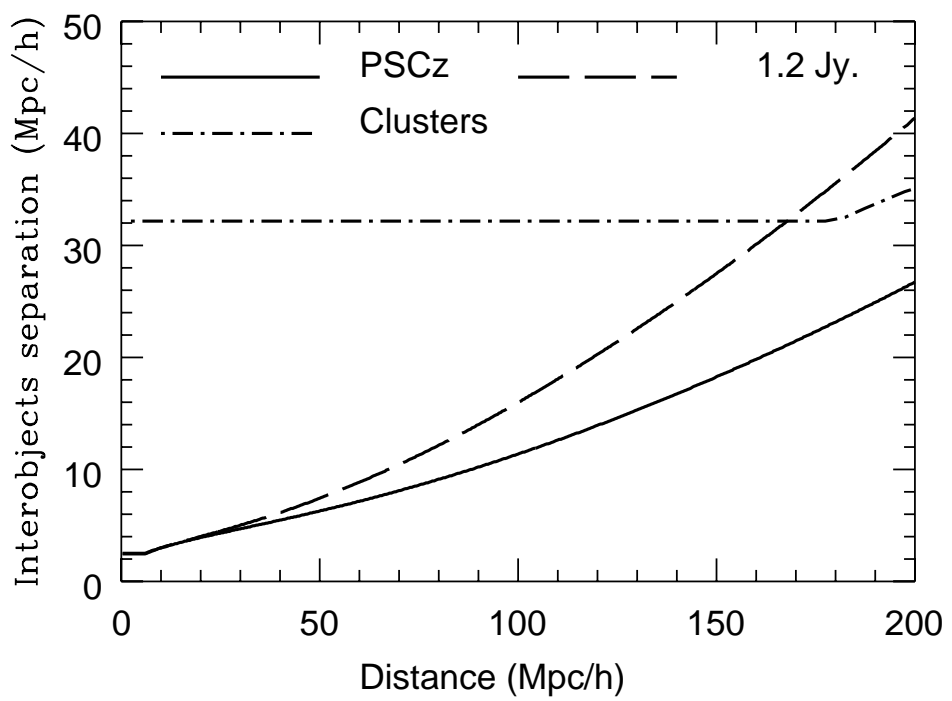
**Figure 19** The amplitude (left) and direction (right) of the cumulative bulk velocity vector. The bottom–left panel refers to the total velocity and the top–left panel to the SGY–component only. The filled triangles show the bulk velocity measured in the Mark III catalogue and the filled square the bulk velocity measured in the SFI catalogue. The grey triangle shows the bulk flow inferred from a survey of 44 Type Ia supernovae by Riess, Press & Kirshner (1995) while the grey square gives the bulk velocity derived by Lauer & Postman (1994) from a survey of brightest cluster galaxies. The dot–dashed lines bracket the  $1-\sigma$  range of the bulk velocity predicted from the PSC $z$  gravity field using Method 1 corrected to include the effect of long-wavelength modes. In the lower panel the model predictions are normalized to  $\beta = 0.76$ , while in the upper panel they are normalized to  $\beta = 0.55$ . In the right-hand panel, the

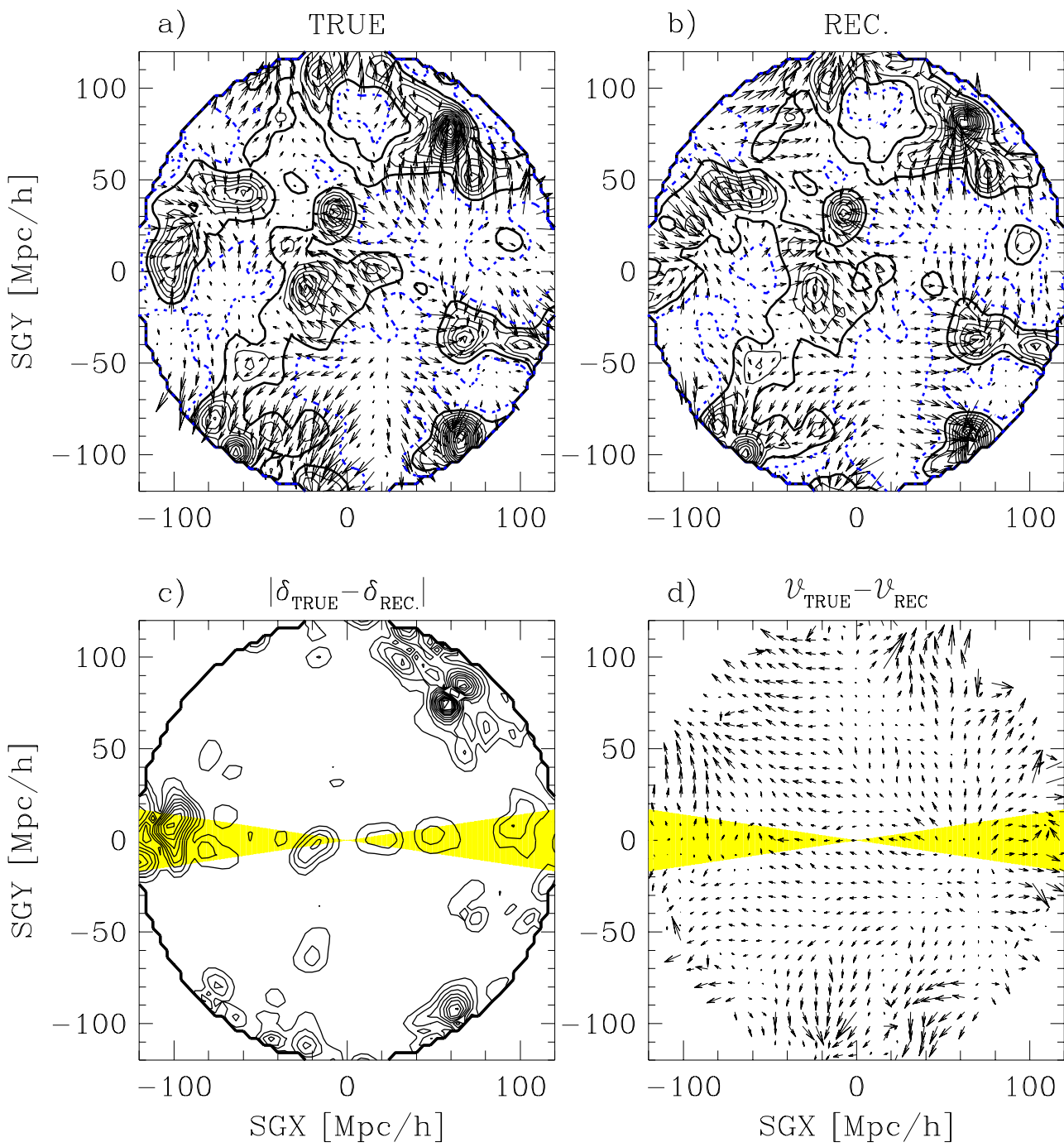
asterisk marks the direction of the CMB dipole in galactic coordinates and the filled circle the direction of the bulk velocity at  $50h^{-1}$  Mpc obtained from the corrected Method 1 and the PSCz survey. The other symbols correspond to those in the left-hand panel, to a distance of  $50 h^{-1}$  Mpc in the case of the Mark III catalogue.

This figure "fig1.gif" is available in "gif" format from:

<http://arxiv.org/ps/astro-ph/9901366v1>







This figure "fig5.gif" is available in "gif" format from:

<http://arxiv.org/ps/astro-ph/9901366v1>

